LOS Rate Estimation in Strapdown Seekers Using Kalman Based Filters

Thesis submitted for the partial fulfillment of the requirement of the degree of

Master in Electrical Engineering (Control System)

Submitted by

Sindhunil Bhaumik

Class Roll Number: 002010802003

Registration Number: 127560 of 2014-2015

Examination Roll Number: M4ELE22003

Under The Guidance of

Prof. Smita Sadhu

Electrical Engineering Department

Faculty Council of Engineering and Technology

Jadavpur University

Kolkata-700032

June 2022

JADAVPUR UNIVERSITY

Kolkata-700032

Certificate of Recommendation

This is to certify that **Mr. Sindhunil Bhaumik (002010802003)** has completed his dissertation entitled, **"LOS Rate Estimation in Strapdown Seekers Using Kalman Based Filters"**, under the direct supervision and guidance of **Prof. Smita Sadhu**, Electrical Engineering Department, Jadavpur University. We are satisfied with his work, which is being presented for the partial fulfillment of the degree of **Master in Electrical Engineering** of Jadavpur University, Kolkata-700032.

Sadhu 24.06.2022

Dr. Smita Sadhu

Professor, Electrical Engineering Department
Jadavpur University, Kolkata-700032

Professor
Electrical Engineering Department
JADAVPUR UNIVERSITY
Kolkata - 700 032

Saswati Mazumdar 24.6.22

Prof. Saswati Mazumdar

Head, Electrical Engineering Department
Jadavpur University, Kolkata-700032

Head
Electrical Engineering Department
JADAVPUR UNIVERSITY
Kolkata - 700 032

Mazumdar 27/6/2022

Prof. Chandan Mazumdar

Dean, Faculty of Engineering and Technology
Jadavpur University, Kolkata-700032

DEAN
Faculty of Engineering & Technology
JADAVPUR UNIVERSITY
KOLKATA-700 032

Faculty Council of Engineering and Technology

JADAVPUR UNIVERSITY

Kolkata-700032

Certificate of Approval

The foregoing thesis is hereby approved as a creditable study of Master in Electrical Engineering and presented in a manner satisfactory to warrant its acceptance as a pre-requisite to the degree for which it has been submitted. It is understood that, by this approval the undersigned does not necessarily endorse or approve any statement made, opinion expressed, or conclusion therein but approve this thesis only for the purpose for which it is submitted.

Final Examination for Evaluation of the Thesis

.....

.....

Signature of Examiners

*Only in case the thesis is approved

Declaration of Originality and Compliance of Academic Ethics

I hereby declare that this thesis contains a literature survey and original research work by the undersigned candidate, as part of his Master of Electrical Engineering Studies.

All information in this document has been obtained and presented in accordance with academic rules and ethical conduct.

I also declare that, as required by these rules and conduct, I have fully cited and referenced all material and results that are not original to this work.

Name: Sindhunil Bhaumik

Examination Roll No.: M4ELE22003

Thesis Title: LOS Rate Estimation in Strapdown Seekers Using Kalman Based Filters

Signature Sindhunil Bhaumik.

ACKNOWLEDGEMENTS

I sincerely thank my supervisor, Prof. Smita Sadhu, Department of Electrical Engineering, Jadavpur University, Kolkata, for her invaluable guidance, suggestions, encouragement, and constant support throughout my thesis work, which helped me in successfully completing it.

I especially thank Prof. Tapan Kumar Ghoshal, Jadavpur University Kolkata for his innovative discussions, and for sharing his valuable suggestions, ideas and thoughts, which inspired me to do a project in this domain as well as helped me throughout my thesis work.

I am also thankful to my classmates for their continuous help and support.

Finally, I would like to thank my parents Mr. Soumendra Nath Bhaumik and Mrs. Krittika Bhaumik and my friends for their unconditional support and love.

Sindhunil Bhamik
Jadavpur University, Kolkata

Date:

ABSTRACT

This dissertation is about the study of Line of Sight (LOS) rate extraction in strapdown seekers using Kalman-like filters. The strapdown seekers are permanently attached to the missile's body. Consequently, the seeker measurements are linked to the motion of the body. Filtering and estimation techniques are required to decouple the measurements from the body attitude motion. The motivation for the study had been the on-going initiatives of designing a more efficient and robust Kalman based filter that can compensate any kind of nonlinear disturbances and noise levels and estimate the important states of the system correctly.

For proper modelling of the strapdown seeker, a substantial knowledge of seeker, seeker guidance and track system is needed. Accordingly, a thorough and deep literature survey has been carried out covering (a) the overview of missile subsystems (b) strapdown seekers (c) estimation methods. The seeker model has been discussed along with the derivation of the guidance loop and the parasitic loops created by the radome error and beam pointing error and their effects on the stability of the system has also been discussed.

For the estimation of seeker signals, the Extended State Kalman Filter (ESKF) has been built, supported with necessary simulations in MATLAB. Accordingly, the work of Lin [1] has been verified and the algorithm has been tested for some different disturbance input conditions. Moreover, a comparative study between the ESKF and the conventional EKF has also been carried out with the help of relevant simulations in MATLAB. To prove the utility of ESKF, it has been implemented in a missile-target interception problem originally tackled with an adaptive EKF method by Madyastha[2]. Finally a robustness analysis has been performed for the ESKF by testing the filter with different noise levels and observing the MSE waveforms with the help of MATLAB simulations.

Contents

List of Symbols

q_t	True LOS angle
q^*	Apparent LOS angle
q_s	Seeker dish angle
$\hat{q}$	Estimated LOS angle
a_{MC}	Acceleration command
a_M	Missile acceleration
ν	Body attitude angle
$\dot{\nu}$	Body moving rate
R	radome Slope
N	Navigation gain
V_c	Missile-target closing velocity
T_g	Guidance system time constant
T_α	Turning rate time constant
V_m	Missile velocity
η	Radome refraction angle
θ_B	Seeker gimbal angle
θ_{BC}	Beam angle control command
P	Beam control code

R^*	Beam pointing error slope
K	Seeker forward loop gain
$\dot{v}_m$	Angular velocity of the body measured by IMU
K_g	Angular rate gyro scale
$F(\Delta\theta_{BC})$	Beam control unit
$G(\theta_{BC})$	large Beam control unit
$\Delta\phi_{BC}$	Reading element phase shift value
V_M	Tangential veocity of the missile
V_T	Tangential velocity of the target
a_T	Normal acceleration of the target
θ_M	Flight path angle of the missile
θ_T	Flight path angle of the target
g	Acceleration due to gravity

List of Figures

Abbreviations

LOS	Line of Sight
ESKF	Extended State Kalman Filter
EKF	Extended Kalman Filter
MSE	Mean Squared Error
FOV	Field of View
PNG	Proportional Navigation Guidance
SMG	Sliding Mode Guidance
UKF	Unscented Kalman Filter
DRE	Disturbance Rejection Effect
ESO	Extended State Observer
PBT	Phantom Bit Technology
SNR	Signal to Noise Ratio
IMU	Inertial Measurement Unit
PARS	Phased Array Radio Seeker
APN	Augmented Proportional Navigation

Chapter 1

Introduction

1.1 History and Background

Missiles have been in use from as early as the Vedic period in India. Since that time, Indian warriors have employed *"Astras"* as projectiles in various forms. In the war of Srirangapatna (1972), the army of Tipu Sultan used thousands of rockets against the British colonial army, resulting in their defeat. Spears made of bamboo or steel were used as rockets and were propelled by cannon powder, which was compressed in a cast iron cylinder with a nozzle and igniters and capable of assaulting enemy soldiers.

In the twentieth century, it can be safely said that the technology of guided missiles has seen contribution from several fields of science; As a result, approving the first efforts i.e. the innovation of the guided missiles to any single inventor or any one group of experimenters is nearly impossible. The first guided missile, in the most literal sense, relied on human muscle strength and ocular guidance. For the sake of completeness of this discussion, in the twentieth century, Professor A. M. Low is credited with developing the earliest guided missile. [3]. He started experiments with small-scale pilotless aircrafts fueled by internal combustion engines in 1914, with the assistance of his British expertise. For the purpose of guidance, a basic time-switching mechanism for radio commands was implemented.. Multiple flights were carried out in 1916 and 1917, but the absence of an autopilot prevented successful performance.

During World War I, the use of guided missiles came to the spotlight [4]-[8]. The origins of today's missiles can be traced back to Germany. The very first guided missiles V1 and V2 were developed by the country and were utilized

against actual military targets in World War II. Inspired by the Germans, by the end of the war, other nations were developing equivalent guided missiles. Several distinct guidance systems were successfully developed by the United States during the course of World War II for automatically and remotely directing the flight paths of bombs [3] [9] [10]. From that time, a lot of research work and developmental efforts have been paid out over the whole field of guided missiles. The Karman group during that time developed rockets powered by solid-fuels and liquid-fuels. Karman and his group designed JATO rocket. A solid fuel rocket named "Private" was developed later. Also, "Corporal", the liquid fuel rocket was designed afterwards. A modified version of V-1 named "The Loon" was used for testing components of guided missiles [11]. Currently, the USA leads the field of guided missile technology followed by Russia, UK, China and France. Along with that, the USA, currently controls the fastest missile named "Minuteman III" that can travel 10,000 km at 15,000 mph.

Since its independence, India has researched, developed, and deployed a variety of tactical and strategic missile systems. Over time, all types of missile systems have been developed, including cruise, ballistic, anti-ship, air-to-air, air-defence, and anti-missile systems. India is one of four nations in the world having anti-ballistic missile defence systems. Defence Research and Development Organisation (DRDO) successfully developed a short small range surface-air missile named *Trishul*. It is equipped with a warhead weighing 15 kg and has a range of 12 km. A medium ranged mobile surface to air missile *Akash* was also created by DRDO [12]. The missile can aim at cruise missiles, aircrafts and ballistic missiles up to 30 km to 60 km distance and at heights up to 18,000 m. The *Nag* missile, which is also known as "Prospina" which is used for land-attack, is an Indian all-weather, third generation, anti-tank, lock-on after launch guided missile (ATGM) having a range of operation of 500 m to 20 km. It has a ten-year, maintenance-free shelf life and a probability of one-shot hit of 90%. *Prithvi, Prahaar* and *Pralay* missiles were developed as tactical surface to surface ballistic short range missiles. With the advancement of technology, the *Agni-I*, *Agni-II*, and *Agni-III* missiles were developed. In the early 2010s, separate programmes called *Agni-IV* and *Agni-V* having intercontinental ranges and MIRV came out.

1.2 Classification of Missiles

There are two types of missiles that can be broadly classified: *(1) Unguided Missiles* and *(2) Guided Missiles*. They are discussed below in brief.

1.2.1 Unguided Missiles

An unguided missile lacks the presence of any control or guidance system. The accuracy of such missiles is decided by the launching platform, i.e., the operator and simple laws of physics [13]. The small wings also help to determine their trajectory and accuracy. The main advantage of unguided missiles is that they are very affordable to make but they lack the precision of a guided missile [14]. These missiles reside in the *strategic* missile class [15]. Examples of unguided missiles are the FFAR, FROG-7, The Hydra 70, Little John and Honest John.

1.2.2 Guided Missiles

Guided missiles are unmanned vehicles for which the flight path can be controlled with different guidance mechanisms to increase the precision with which the target is hit. The incorporation of an energy source to provide the requisite power for movement (propulsion), intelligence to travel in the proper direction (guidance), and successful manoeuvring (control) are the major technologies driving the guidance missiles. Although guided missiles are expensive to make, they beat the unguided missiles on the ground of precision and accuracy. The various parts of a guided missile are: Firstly, the air frame and control surfaces, i.e. the body of aircraft; secondly, the propulsion system, i.e. system required to generate the movement of the missiles; thirdly, the warhead system and finally the guidance mechanism and control system.

1.3 Seekers and their classifications

A missile's seeker is one of its most crucial components. Seekers are the systems used in missiles to lead them on the right trajectory to accurately hit the desired targets. The seeker essentially computes a fire control solution for the missile by delivering guidance signals to the autopilot. The seeker consists of a sensor by which it can detect and track targets in the outside world; in the case of RF seekers, this sensor is the antenna. IR guided and TV guided missiles make use of camera-type sensors. RF seekers commonly use monopulse antennas. These are antennas that have a compound feed, and essentially provide the seeker immunity to early types of angle deception jamming, such as amplitude modulation. From the constructional point of view, there are two popular categories of seekers extensively in use- gimbaled seeker and strapdown seeker.

1.4 Strapdown Seeker

In the past few years, strapdown seekers are replacing traditional gimbaled seekers in a fast pace. A gimbaled seeker is supported by a separate platform attached to the body of the missile and it is balanced by the gimbaled system. A strapdown seeker, on the other hand, is permanently attached to the missile's body. The strapdown seeker has a significant disadvantage over a gimbaled seeker. The strapdown seeker's field of view (FOV) is narrower compared to its gimbaled counterpart which may lead to larger miss distance. Moreover, this seeker can only measure LOS data in relation to body coordinates. Hence, its measurement is combined with the motion of missile's body, as it is permanently fixed to the body. However, the implementation of strapdown seekers is more economic and simple as compared to the gimbaled seekers and for this reason, strapdown seekers have found extensive use in the guidance systems in recent years.

1.5 Outline of Thesis

In Chapter 1, a quick summary of the missiles, seekers and their classifications along with the history and background has been discussed.

In Chapter 2, a thorough literature survey is done on the seekers. Emphasis on the strapdown seekers has been given along with all the corresponding and necessary research works that had been carried out in the past few years. A brief literature survey on the filtering and estimation methods has also been discussed.

In Chapter 3, the Extended State Kalman Filter (ESKF) has been thoroughly discussed with a detailed derivation of the algorithm

In Chapter 4, the seeker model has been discussed. All the individual components of the guidance loop has been discussed briefly and finally, the effect of the parasitic loops on the guidance loop stability has been talked about.

In Chapter 5, the ESKF algorithm has been applied for the seeker signal estimation. Various simulations have been performed with the help of MATLAB showing the estimated states and the inputs.

In Chapter 6, the conventional EKF algorithm for unknown inputs has been discussed and a comparative study between the ESKF and the EKF has been

conducted along with the necessary simulations in MATLAB.

In Chapter 7, the ESKF method has been applied to a different missile-target interception problem. Two different types of input waveforms have been considered for the simulation purpose.

In Chapter 8, the robustness analysis of the ESKF has been performed. Different noise levels have been considered and the mean squared estimation errors have been plotted in MATLAB.

Chapter 9 concludes the whole thesis work and also provides direction for future research in this domain.

Chapter 2

Literature Survey

2.1 Overview of Missile Subsystems

The missile system broadly consists of two subsystems [16, 17]: the guidance system and the control system. In guidance and control system, several underlying concepts of servomechanism are used [18, 19, 20]. Servomechanism is essentially an automatic electro-mechanical device that uses an error sensing negative feedback. The principal goal of servomechanism is to cut down the error present in the control system. For missile system, the intention of the guidance part is to develop the desired course to the target, also treated as an input signal. The output of the guidance system is the actual missile path. The error signal, delivered to the control system, is the difference between the preferred and true flight path. The control system changes the position of the missile depending on the desired course to target. Hence, the essential goal of the guidance system is to dig up and track the target by determining the missile's flight route. The seeker collects the necessary information by measuring the LOS rate and accordingly sends the data to the computers to generate the control signals. The control surface servos operate using the output voltages, which we get from the information generated [21].

2.2 Strapdown Seekers

In the past few years, strapdown seekers have gained much popularity as compared to the traditional gimbaled seekers mainly for economic reasons. With this growing popularity, several studies have been conducted on various technical aspects of strapdown seekers. These studies can be broadly classified into several directions. Some studies have been carried out investigating the effects of scale

factor errors on guidance loop [22]-[25]. Some studies were devoted to the analysis of the stability regions of the parasitic loops that are being created inside the homing guidance loop due to these errors [26]-[29]. Another research direction includes devising new guidance laws for terminal homing guidance loops in case of strapdown seekers [30]-[32]. As discussed earlier, the strapdown seeker's FOV is smaller as compared to the gimbaled seeker[33, 34]. In view of this problem, Lee [35] devised a guidance law to ensure that missiles having small field-of-view strapdown seekers retain lock-on states till the target is intercepted.

The Proportional Navigation Guidance (PNG) law depending on the LOS rate has been used by most modern homing missiles [36]-[39]. Unlike many other guidance laws, PNG law is very simple to implement [40][41]. Xin[42] developed a guidance law based on the nonlinear optimal control problem using the seeker FOV as a constraint. Sang[43] designed a switching logic that toggles amidst an original PNG law and a guidance law that maintains the seeker's look angle at a specific FOV limit during the homing period. Lee[35]) proposed a guidance law combining two different guidance laws- a conventional PNG law and a Sliding Mode Guidance (SMG) law to maintain the lock-on condition between the missile and the target.

2.3 Estimation Methods

In case of strapdown seekers, the measurements are coupled with the body attitude motion. As a result, an algorithm is required to decouple the motion of the body and to predict LOS information accurately [44]. In recent years, several studies on the computation of LOS data for the strapdown seekers have been performed. This process essentially requires a noise filter that can effectively extract the LOS information from the missile body motion. Kalman Filter is a great tool to obtain the optimal estimation in case of linear system in the presence of white Gaussian noise. However, simple Kalman Filter is inapplicable in case of nonlinear systems. To eradicate this problem, Extended Kalman Filter (EKF) has been developed which expands the dynamic model of a nonlinear system as a Taylor series about the current state estimate and performs the linearization by neglecting the higher order terms. Due to the linearization, EKF faces some drawbacks which include decreased estimation precision, complexity in calculation of the Jacobian matrix, implementation problems etc [45]. To handle these problems, S.J. Julier proposed the Unscented Kalman Filter (UKF) for performing state prediction more accurately [46]. A collection of sigma points is selected to represent the

mean and variance of a random variable, and each point is incarnated using a nonlinear model, from which the predicted mean and covariance can be derived straight away. [45]. Unlike the EKF which can obtain only a first order precision, the UKF can provide upto third order precision for Gaussian random variables [45].

Jang[34] took the time delay of the guidance filter in consideration and proposed a guidance algorithm to predict the LOS data for short-range missiles with strapdown seekers. Zhang[47] approximated the LOS rate using a UKF to deal with the strapdown imaging guidance system's large nonlinearity and substantial measurement noise. The outcomes were compared with those of an EKF to prove its superiority. Sadhu[48] proposed a method that uses a disturbance observer to extract the LOS information. For solving the Disturbance Rejection Effect (DRE) presented by the strapdown seeker, a unique online prediction and correction mechanism was presented by Lin[1] using EKF. The authors used this method to estimate radome and beam pointing error slopes to predict the LOS data. Wang[49] proposed an idea for the extraction of LOS data using nonlinear Tracking-Differentiator and UKF to overcome the difficulties of coupling of measurement system with body attitude motion of strapdown guidance system. Wang[44] created an EKF-based method for predicting the LOS data of a strapdown seeker, as well as a hardware in loop simulation platform to test it. Also, the authors have compared the results with that of a conventional gimbaled seeker. Waldermann[50], using the EKF model and its estimations, suggested a control law based on feedback linearization to decouple missile body motion from seeker motion. Seeker dynamics and control are then combined into a dynamic model that is driven by PNG.

Chapter 3

Overview of the Extended State Kalman Filter

3.1 Introduction

Kalman filtering is among the most extensively utilised techniques in several sectors of research and engineering such as guidance, navigation and control of aircrafts and vehicles, robotic motion planning and control, time series analysis for econometrics and signal processing, trajectory optimization etc. It is an algorithm that takes into account the statistical noises and other inaccuracies and makes use of a series of measurements over time and creates unknown variable estimates which are more accurate than the ones developed from a single measurement alone. The principle of the original KF algorithm is basically the minimization of the mean squared estimation error for linear systems with an accurate model contaminated with white Gaussian noise. Substantial developments have been proposed to the basic KF to deal with more complex filtering problems. To deal with nonlinear systems corrupted with Gaussian noises, the EKF is developed. The EKF algorithm tackles the nonlinear systems by performing linearization of first order. Similarly, Unscented Kalman Filter (UKF) utilizes sampling and third order linearization for the same. Truly speaking, linearization and parameter optimization are the most common approaches to deal with nonlinearity and unpredictability. These methods have been found to be useful for a wide range of real filtering situations, with minimal errors, but that does not change the fact that they have the following drawbacks when working with nonlinear uncertain situations in general [1].

i) Filters constructed using local linearization may face instability problems in

case of nonlinear systems. In general, the development of linearization-based filters has been predicated on the premise that the noise and initial estimation error are minimal enough to ensure the filter's stability. In practical problems, various external disturbances can be present and the sensor's precision may be finite during the execution of the filter. As a result, such assumptions may turn out to be very optimistic and difficult to satisfy. In conclusion, such filters' performance can be particularly vulnerable to early estimating inaccuracy and noise..

ii) Traditional KF algorithms operate by minimising a specific index depending on the worst-case uncertainty bound. This unavoidably necessitates a low enough uncertainty bound; otherwise, the optimization outcome may be conservative. However, when unmodelled dynamics is included in the problem along with the linearization error, this assumption gets critical.

The above problems give rise to the requirement to design an effective, flexible and resilient filter that is capable of dealing with large uncertainties and strong nonlinearities. This is where Extended State Observer (ESO) comes in. The nonlinear uncertainty is handled by ESO as a time-dependent signal that must be assessed and adjusted for, irrespective of the complexity of the uncertain dynamics. The nonlinear and unpredictable dynamics can be considered to be a slowly varying signal as compared to the noise present in the system. To deal with the issues caused by the linearization and worst-case optimization frames, Bai [51] utilized the extended state design to tackle the uncertainty and the nonlinearity. Moreover, the authors optimized the gain of the ESO to develop the Extended State Kalman Filter (ESKF). To show the filter's usefulness, a generic category of nonlinear uncertain time varying systems has been discussed. The derivation of ESKF discussed in the next section has been taken from Bai [51]. Let us now proceed towards the derivation of the filter.

3.2 Problem formulation and design of ESKF

Let us analyse the category of nonlinear time dependent unpredictable systems described by-

$$X_{k+1} = \tilde{A}_k X_k + \tilde{B}_k F(X_k, k) + w_k, \tag{3.1}$$

$$Z_k = \tilde{C}_k X_k + n_k. \tag{3.2}$$

Here $X_k \in \mathbb{R}^n$ is the state vector, $\tilde{A}_k \in \mathbb{R}^{nxn}$, $\tilde{B}_k \in \mathbb{R}^{nxl}$ and $\tilde{C}_k \in \mathbb{R}^{mxm}$ are time-dependent matrices. $F(X_k,k) \in \mathbb{R}^l$ is the system's nonlinear, unpredictable dynamics. $w_k \in \mathbb{R}^n$ and $n_k \in \mathbb{R}^m$ are, respectively, the process noise and measurement noise vectors. $Y_k \in \mathbb{R}^m$ is the output vector and $k = 0, 1, 2, ...$

$F(X_k,k)$ It is commonly known as the "total disturbance," which includes both internal and external uncertainty, such as unpredictable parameter fluctuations, unmodelled dynamics, and errors caused by discretization [51]. The unknown dynamics are separated into three sections in the mathematical model. $\tilde{A}_k \in \mathbb{R}^{nxn}$ is the known linear component, $F(X_k,k)$ is the slowly varying unpredictable dynamics and $w_k \in \mathbb{R}^n$ and $n_k \in \mathbb{R}^m$ are the noises which can have high frequency components [51]. Taking $F(X_k,k)$ as an extended state, It is possible to convert the mathematical model into

$$\begin{bmatrix} X_{k+1} \\ F_{k+1} \end{bmatrix} = A_k \begin{bmatrix} X_k \\ F_k \end{bmatrix} + B_k H_k + \begin{bmatrix} w_k \\ 0 \end{bmatrix}, \tag{3.3}$$

$$Z_k = C_k \begin{bmatrix} X_k \\ F_k \end{bmatrix} + n_k, \tag{3.4}$$

where,

$$F_k = F(X_k,k); H_k = F_{k+1} - F_k; A_k = \begin{bmatrix} \tilde{A}_k & \tilde{B}_k \\ 0 & I \end{bmatrix}; B_k = \begin{bmatrix} 0 \\ I \end{bmatrix}; C_k = \begin{bmatrix} \tilde{C}_k & 0 \end{bmatrix}. \tag{3.5}$$

There are certain assumptions that we need to consider before developing the algorithm for system (2.3)-(2.4). They are listed as follows [51].

I. (A_k, C_k) is uniformly observable.

II. $\{w_k\}_0^\infty$ and $\{n_k\}_0^\infty$ are zero-mean uncorrelated random Gaussian sequences and

$$E(n_k n_k^T) \leq R_k, \tag{3.6}$$
$$E(w_k w_k^T) \leq S_k, \tag{3.7}$$

where $\{R_k\}_0^\infty$ and $\{S_k\}_0^\infty$ are known sequences which are bounded uniformly. Additionally, $\{w_k\}_0^\infty$, $\{n_k\}_0^\infty$ and X_0 are mutually exclusive.

III.

$$E(\begin{bmatrix} X_0 - \hat{X}_0 \\ F_0 - \hat{F}_0 \end{bmatrix} \begin{bmatrix} X_0 - \hat{X}_0 \\ F_0 - \hat{F}_0 \end{bmatrix}^T) \leq P_0, \tag{3.8}$$

where $\hat{X}_0$ is the estimate of X_0 and P_0 is a constant matrix which is previously known.

IV.

$$E(H_{k,j}^2) \leq \tilde{q}_{k,j}, \quad j = 1,2,...,l, \quad \forall k \geq 0 \tag{3.9}$$

where $\{q_{k,j}\}_0^\infty$ is uniformly bounded and known sequence.

The assumption *I* is a fundamental assumption that ensures the stability of Kalman filters. According to the assumptions *III* and *IV*, the prediction error for the starting state and unknown dynamics and the variation of the function $F(.)$ between neighbourhood time steps are bounded [1]. The size of the evolving nonlinear uncertain function $F(.)$ is represented by $\bar{q}_k$. Now, let us design the extended state observer (ESO) based on (2.3)-(2.4) as follows.

$$\begin{bmatrix} \hat{X}_{k+1} \\ \hat{F}_{k+1} \end{bmatrix} = A_k \begin{bmatrix} \hat{X}_k \\ \hat{F}_k \end{bmatrix} + B_k \hat{H}_k - K_k(Z_k - C_k \begin{bmatrix} \hat{X}_k \\ \hat{F}_k \end{bmatrix}), \tag{3.10}$$

where, $\hat{H}_k$ is the estimate of H_k, which is utilised to rectify the state's prediction error and uncertainty by utilising all model information. Hence, we use the nominal model of H_k as

$$\tilde{H}_k = \tilde{F}(X_{k+1}, k+1) - \tilde{F}(X_k, k). \tag{3.11}$$

and the estimate of $\tilde{H}_k$ is given as

$$\hat{\tilde{H}}_k = \tilde{F}(\tilde{A}_k \hat{X}_k + \tilde{B}_k \hat{F}_k, k+1) - \tilde{F}(\hat{X}_k, k). \tag{3.12}$$

Depending upon the nominal estimate, $\hat{H}_k$ can be defined as

$$\hat{H}_{k,j} = sat(\hat{\tilde{H}}_{k,j}, \sqrt{\tilde{q}_{k,j}}), \quad j = 1, 2, ..., l. \tag{3.13}$$

where $sat(.)$ denotes the saturation function which is given by

$$sat(f, x) = max\{min\{f, x\}, -x\}, \quad x > 0.$$

The saturation function is employed to ensure that $\hat{H}_{k,j}$ is confined. Also, $\hat{H}_{k,j}$ is the j^{th} element of vector $\hat{H}_k$. Since the system is contaminated with noise and unpredictability, the regulation of K_k is a necessary trade-off between the disturbance dismissal and the noise sensitivity. Thus unlike the case of ESO, K_k becomes dynamic and manually regulated. Rather, optimization is performed to minimize the mean square error and the optimal kalman gain K_k is computed for each step [51]. The estimation error of ESKF is denoted as

$$e_k = \begin{bmatrix} X_k \\ F_k \end{bmatrix} - \begin{bmatrix} \hat{X}_k \\ \hat{F}_k \end{bmatrix}. \tag{3.14}$$

Replacing k with $(k+1)$, we get

$$e_{k+1} = \begin{bmatrix} X_{k+1} \\ F_{k+1} \end{bmatrix} - \begin{bmatrix} \hat{X}_{k+1} \\ \hat{F}_{k+1} \end{bmatrix}. \tag{3.15}$$

From (2.4) and (2.15), we get

$$
\begin{aligned}
e_{k+1} &= \begin{bmatrix} X_{k+1} \\ F_{k+1} \end{bmatrix} - \begin{bmatrix} \hat{X}_{k+1} \\ \hat{F}_{k+1} \end{bmatrix} \\
&= A_k \begin{bmatrix} X_k \\ F_k \end{bmatrix} + B_k H_k + \begin{bmatrix} w_k \\ 0 \end{bmatrix} - A_k \begin{bmatrix} \hat{X}_k \\ \hat{F}_k \end{bmatrix} - B_k \hat{H}_k + K_k (Z_k - C_k \begin{bmatrix} \hat{X}_k \\ \hat{F}_k \end{bmatrix}) \\
&= A_k \begin{bmatrix} X_k \\ F_k \end{bmatrix} + B_k H_k + \begin{bmatrix} w_k \\ 0 \end{bmatrix} - A_k \begin{bmatrix} \hat{X}_k \\ \hat{F}_k \end{bmatrix} - B_k \hat{H}_k + K_k (C_k \begin{bmatrix} X_k \\ F_k \end{bmatrix} + n_k - C_k \begin{bmatrix} \hat{X}_k \\ \hat{F}_k \end{bmatrix}) \\
&= A_k (\begin{bmatrix} X_k \\ F_k \end{bmatrix} - \begin{bmatrix} \hat{X}_k \\ \hat{F}_k \end{bmatrix}) + B_k (H_k - \hat{H}_k) + \begin{bmatrix} w_k \\ 0 \end{bmatrix} + K_k C_k (\begin{bmatrix} X_k \\ F_k \end{bmatrix} - \begin{bmatrix} \hat{X}_k \\ \hat{F}_k \end{bmatrix}) + K_k n_k \\
&= (A_k + K_k C_k)(\begin{bmatrix} X_k \\ F_k \end{bmatrix} - \begin{bmatrix} \hat{X}_k \\ \hat{F}_k \end{bmatrix}) + B_k (H_k - \hat{H}_k) + K_k n_k + \begin{bmatrix} w_k \\ 0 \end{bmatrix}.
\end{aligned}
$$

Using (2.14) and simplifying, we arrive at

$$
e_{k+1} = (A_k + K_k C_k) e_k + K_k n_k + B_k (H_k - \hat{H}_k) + \begin{bmatrix} w_k^T & 0 \end{bmatrix}^T. \tag{3.16}
$$

Denote $\bar{H}_k = (H_k - \hat{H}_k)$. The expected value of the mean squared error of ESKF can be given as

$$
\begin{aligned}
E[e_{k+1} e_{k+1}^T] = E[((A_k + K_k C_k) e_k + K_k n_k + B_k (H_k - \hat{H}_k) + \begin{bmatrix} w_k^T & 0 \end{bmatrix}) \\
((A_k + K_k C_k) e_k + K_k n_k + B_k (H_k - \hat{H}_k) + \begin{bmatrix} w_k^T & 0 \end{bmatrix})^T].
\end{aligned}
$$

Simplifying the right hand side, we can write

$$E[e_{k+1}e_{k+1}^T] = (A_k + K_kC_k)E[e_ke_k^T](A_k + K_kC_k)^T + K_kE[n_kn_k^T]K_k^T + E[\bar{H}_k\bar{H}_k^T] + \begin{bmatrix} E[w_kw_k^T] & 0_{nxl} \\ 0_{nxl} & 0_{lxl} \end{bmatrix} + E[(A_k + K_kC_k)e_k\bar{H}_k^T] + E[\bar{H}_ke_k^T(A_k + K_kC_k)^T].$$

The above result follows from the assumption that n_k, w_k and e_k are uncorrelated or mutually independent. Now, from the Young's inequality in case of matrices [51], we can write

$$(H_k - \hat{H}_k)(H_k - \hat{H}_k)^T \leq 2H_kH_k^T + 2\hat{H}_k\hat{H}_k^T.$$

Next we shall use the assumption A4 that indicates the boundness of H_k. Using A4, the above inequality can be expressed as

$$\begin{aligned}(H_k - \hat{H}_k)(H_k - \hat{H}_k)^T &\leq 2l.diag(\begin{bmatrix} H_{k,1}^2 & H_{k,2}^2 & \dots & H_{k,l}^2 \end{bmatrix}) \\ &\quad + 2l.diag(\begin{bmatrix} \hat{H}_{k,1}^2 & \hat{H}_{k,2}^2 & \dots & \hat{H}_{k,l}^2 \end{bmatrix}) \qquad (3.17) \\ &\leq 4l.diag\begin{bmatrix} \tilde{q}_{k,1} & \tilde{q}_{k,2} & \dots & \tilde{q}_{k,l} \end{bmatrix}. \qquad (3.18)\end{aligned}$$

Let us now design two important matrices given by

$$Q_{1,k} = \begin{bmatrix} 0_{nxn} & 0_{nxl} \\ 0_{lxn} & 4\tilde{Q}_k \end{bmatrix} \quad and \quad \tilde{Q}_k = l.diag(\begin{bmatrix} \tilde{q}_{k,1} & \tilde{q}_{k,2} & \dots & \tilde{q}_{k,l} \end{bmatrix}).$$

Thus, it can be followed that

$$E[(H_k - \hat{H}_k)(H_k - \hat{H}_k)^T] \leq 4\tilde{Q}_k; \quad E[\bar{H}_k\bar{H}_k^T] \leq Q_{1,k}. \qquad (3.19)$$

Furthermore, because the noise affecting F_k is related to the noise impacting X_k, the associated terms of e_k and $\bar{H}_k$ cannot be overlooked [51]. From the Young's inequality in case of matrices, the rearmost two terms of the expectation of mean squared error have the upper bound

$$(A_k+K_kC_k)e_k\bar{H}_k^T+\bar{H}_ke_k^T(A_k+K_kC_k)^T\leq\theta(A_k+K_kC_k)e_ke_k^T(A_k+K_kC_k)^T+\frac{1}{\theta}\bar{H}_k\bar{H}_k^T, \tag{3.20}$$

where $\theta>0$. The equality satisfies iff

$$\theta(A_k+K_kC_k)e_k=\bar{H}_k. \tag{3.21}$$

θ is intended to separate the cross terms of prediction error and uncertainties [51] for the sake of simplicity. It is designed as,

$$\theta=\sqrt{\frac{tr(Q_{1,0}}{tr(P_0)}}. \tag{3.22}$$

Let us now design another matrix $Q_{2,k}=\begin{bmatrix}S_k & 0_{nxl}\\ 0_{lxn} & 0_{lxl}\end{bmatrix}$. Now, from assumption A2, we know that $E[w_kw_k^T]\leq S_k$. Hence, we can easily set the upper bound as it follows from A2 that

$$\begin{bmatrix}E[w_kw_k^T] & 0_{nxl}\\ 0_{lxn} & 0_{lxl}\end{bmatrix}\leq\begin{bmatrix}S_k & 0_{nxl}\\ 0_{lxn} & 0_{lxl}\end{bmatrix}$$
$$\text{or, }\begin{bmatrix}E[w_kw_k^T] & 0_{nxl}\\ 0_{lxn} & 0_{lxl}\end{bmatrix}\leq Q_{2,k}.$$

Now, using all the above results, the expected value of the mean squared estimation error satisfies

$$E[e_{k+1}e_{k+1}^T] \leq (A_k + K_kC_k)E[e_ke_k^T](A_k + K_kC_k)^T + K_kR_kK_k^T + Q_{1,k} + Q_{2,k} \\ +\theta(A_k + K_kC_k)E[e_ke_k^T](A_k + K_kC_k)^T + \frac{1}{\theta}Q_{1,k}.$$

Further reducing it, we get,

$$E[e_{k+1}e_{k+1}^T] \leq (1+\theta)(A_k + K_kC_k)E[e_ke_k^T](A_k + K_kC_k)^T \\ + K_kR_kK_k^T + (1+\frac{1}{\theta})Q_{1,k} + Q_{2,k}.$$

Let us assume that P_k fulfils the iteration equation given below.

$$P_{k+1} \leq (1+\theta)(A_k + K_kC_k)P_k(A_k + K_kC_k)^T + K_kR_kK_k^T + (1+\frac{1}{\theta})Q_{1,k} + Q_{2,k}, \tag{3.23}$$

P_0 is the initial value of P_k. In consequence, it can be followed that

$$E[e_ke_k^T] \leq P_k \quad = 0, 1, 2, ... \tag{3.24}$$

According to (2.24), P_k represents the upper limit of the MSE $E[e_ke_k^T]$. Rather than explicitly minimising $E[e_ke_k^T]$ at each time interval, K_k is chosen to minimise P_k. Interpret

$$K_k^* = arg\,min\{(1+\theta)(A_k + K_kC_k)P_k(A_k + K_kC_k)^T + K_kR_kK_k^T\}. \tag{3.25}$$

It is known that the matrices P_k and R_k are positive semi-definite and positive definite respectively. It implies that $(C_kP_kC_k^T + \frac{1}{1+\theta}R_k)$ is positive definite [51]. Thus, it can be followed that

$$(1+\theta)(A_k + K_kC_k)P_k(A_k + K_kC_k)^T + K_kR_kK_k^T$$

$$= (1+\theta)(A_k P_k C_k^T (C_k P_k C_k^T + \frac{1}{1+\theta} R_k)^{-1}) + K_k)(C_k P_k C_k^T + \frac{1}{1+\theta} R_k)$$

$$(A_k P_k C_k^T (C_k P_k C_k^T + \frac{1}{1+\theta} R_k)^{-1} + K_k)^T - (1+\theta) A_k P_k C_k^T (C_k P_k C_k^T + \frac{1}{1+\theta} R_k)^{-1} C_k P_k A_k^T$$

$$+(1+\theta) A_k P_k A_k^T$$

. Hence, it is easy to know

$$K_k^* = -A_k P_k C_k^T (C_k P_k C_k^T + \frac{1}{1+\theta} R_k)^{-1}. \tag{3.26}$$

This is the expression of the optimal Kalman gain that needs to be updated at each step. Combining all the results, the ESKF algorithm may be summarized as follows.

$$\begin{bmatrix} \hat{X}_{k+1} \\ \hat{F}_{k+1} \end{bmatrix} = A_k \begin{bmatrix} \hat{X}_k \\ \hat{F}_k \end{bmatrix} + B_k \hat{H}_k - K_k (Z_k - C_k \begin{bmatrix} \hat{X}_k \\ \hat{F}_k \end{bmatrix}),$$

$$K_k^* = -A_k P_k C_k^T (C_k P_k C_k^T + \frac{1}{1+\theta} R_k)^{-1},$$

$$P_{k+1} = (1+\theta)(A_k + K_k C_k) P_k (A_k + K_k C_k)^T + K_k R_k K_k^T + (1+\frac{1}{\theta}) Q_{1,k} + Q_{2,k},$$

$$Q_{1,k} = \begin{bmatrix} 0_{nxn} & 0_{nxl} \\ 0_{lxn} & 4\tilde{Q}_k \end{bmatrix}, \quad Q_{2,k} = \begin{bmatrix} S_k & 0_{nxl} \\ 0_{lxn} & 0_{lxl} \end{bmatrix}, \quad \tilde{Q}_k = l.diag(\begin{bmatrix} \tilde{q}_{k,1} & \tilde{q}_{k,2} & \dots & \tilde{q}_{k,l} \end{bmatrix})$$

$$\theta = \sqrt{\frac{tr(Q_{1,0}}{tr(P_0)}}, \quad \hat{H}_{k,j} = sat(\hat{\tilde{H}}_{k,j}, \sqrt{\tilde{q}_{k,j}}), \quad \tilde{H}_k = \tilde{H}(\hat{X}_k, k), \quad j = 1,2,...,l,$$

and $sat(.)$ is the saturation function given by $sat(f,x) = max\{min\{f,x\}, -x\}, x > 0$.

ESKF can be thought of as a Kalman based filter tackling nonlinear unpredictable time-dependent systems. However, ESKF differs from the traditional KF type filters on some grounds [51]. They are listed below.

i) Traditional KF uses linearization to resemble the system model as closely as possible. This may result in instability where significant noise and substantial initial error is involved. On the other hand, ESKF assumes the nonlinear uncertainty to be a time dependent signal that needs to be predicted and corrected, irrespective of the complexity of the model. As a result, ESKF bypasses linearization, which might result in divergence and inaccuracy.

ii) In contrast to traditional KF, ESKF solves the optimization using the limit for variable rate of unpredictable dynamics rather than the limit for the unpredictable dynamics itself. This signifies that traditional KF algorithms require the uncertainty to be sufficiently small to ensure acceptable performance while in case of ESKF, the nonlinear unknown dynamics is only assumed to be slowly fluctuating .

iii) The disruptions in ESKF are divided into two categories, slowly changing unpredictable dynamics and rapidly varying noise, and it supports distinct approaches to dealing with these two types of interruptions. The majority of present filtering techniques can only tackle one form of disruption. This makes ESKF more accurate and flexible.

iv) The stability of traditional KF type filters can be guaranteed for little initial prediction error and minor disrupting noise but ESKF works more accurately even if these conditions are not met. It adds an additional state to the filter to actively predict the nonlinear unknown dynamics before compensating for them.

Chapter 4

The Seeker Model

Modelling of missile seeker is one of the most important factors in the estimation of LOS information. In this chapter, we shall discuss about the mathematical modelling of the seeker and the factors affecting it. Two main factors, namely, radome error and beam pointing error will be discussed and the modelling will be done accordingly. Radomes are formations fixed to the heads of missiles consisting of strapdown seekers .A radome's primary function is to relay receiving radar signals without any distortion [1]. Radomes also help to endure the thermal and physical loads that supersonic flight imposes. Radome performs dispersion of electromagnetic waves and hence, gives rise to imperfection in the LOS angle which is called the radome refraction angle [1]. Generally speaking, the refraction angle is usually relatively insignificant, less than 1^o in most cases. However, the angular rate of change of this refraction angle may create major guidance issues because it produces a parasitic loop inside the guidance loop. As a result, a stability problem arises which increases the miss distance.

The strapdown seekers are mounted on the body of the missiles, unlike their traditional gimbaled counterparts. Using the phase shift value of the phase shifter's radiation, the phased array radar seeker accomplishes beam scanning [1]. As a result, the digital phase shifter's effectiveness determines the seeker beam scanning efficiency.Although sophisticated technologies like as Phantom Beat Technology (PBT) improve seeker beam steering efficiency, beam aiming inaccuracy occurs because the seeker employs open-loop control to manage beam pointing [1]. As the beam screening angle goes up, this fluctuates, resulting in insufficient decoupling of missile's physical motion throughout seeker beam scanning. As a result, an additional parasitic loop is established inside the guidance homing loop. The Disturbance Rejection Effect (DRE) problem refers

to the inadequate decoupling effect of the missile physical movement induced by radome and beam pointing errors. [1]. Let us now model the seeker mathematically and incorporate the effect of DRE problem on the existing model.

4.1 The Guidance Loop

Fig. 4.1 depicts a simplified schematic of a guiding loop with radome distortion.

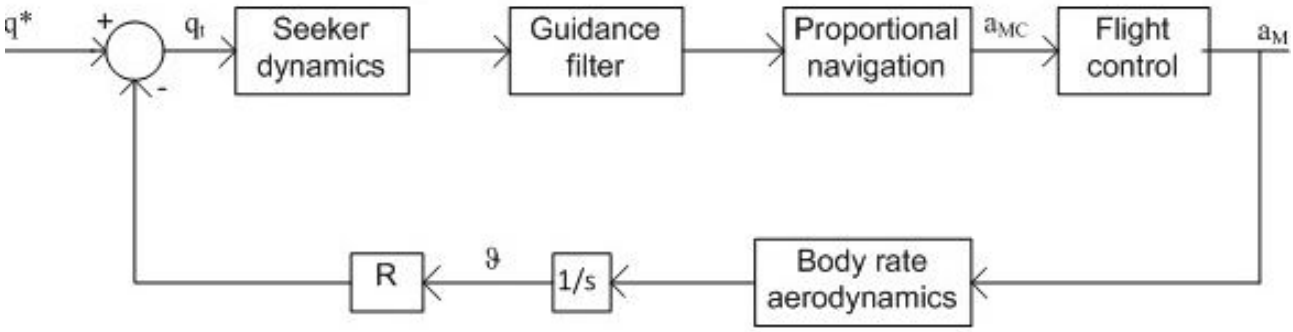

Figure 4.1: Simplified guidance loop

The terminology of the guidance model according to Fig. 4.1 is shown in the following table.

q_t	True LOS angle
q^*	Apparent LOS angle
q_s	Seeker dish angle
$\hat{q}$	Estimated LOS angle
a_{MC}	Acceleration command
a_M	Missile acceleration
ν	Body attitude angle
$\dot{\nu}$	Body moving rate
R	Radome slope

The missile seeker, which follows the target, efficiently measures the LOS data. The measured LOS information is fed to the seeker dynamics and it produces the seeker dish rate information. A noise filter reduces the noise in the radar measurement, resulting in an estimate of the LOS angle. This data is supplied into the

Proportional Navigation (PN) block, which generates an acceleration command for the flight control system.

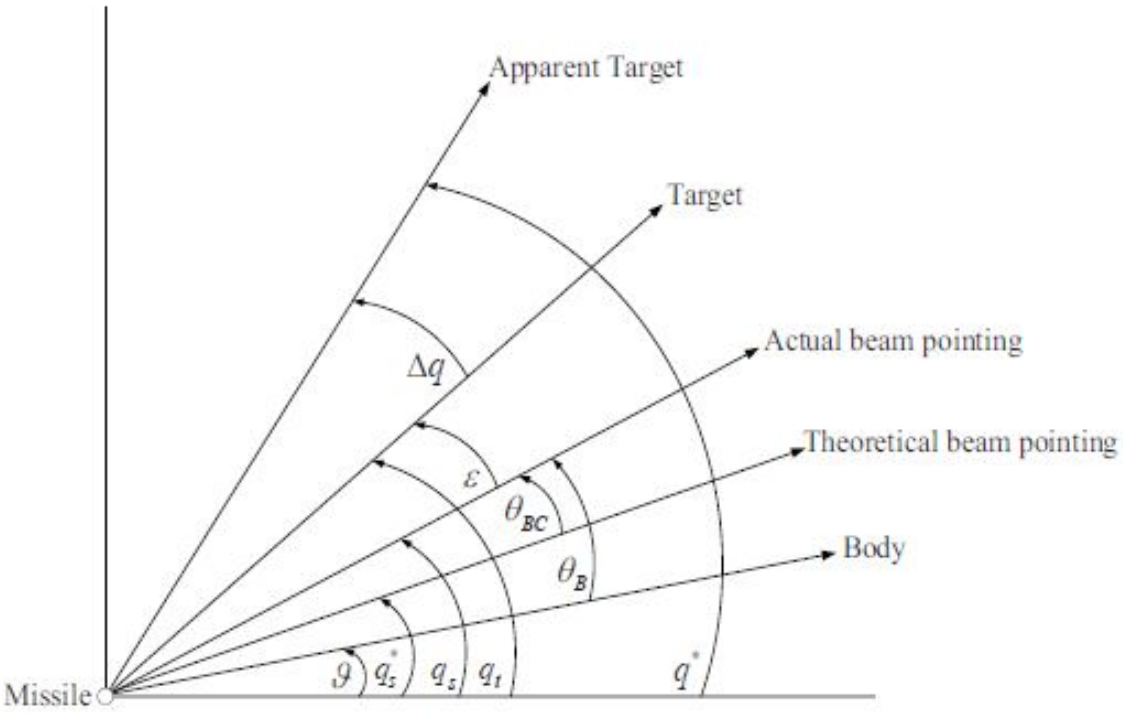

Figure 4.2: The basic missile-target geometry of a strapdown seeker [1]

The flight control system produces the true missile acceleration which, in turn, is fed to the aerodynamics block to get the body moving rate, which, after passing through an integrator produces the body attitude angle. The basic geometric model of the missile and target for strapdown seeker is given in Fig. 4.2. Let us now discuss the function of each block in detail and derive the transfer function model of the system.

4.2 The Proportional Navigation

As a major category of traditional guidance, the proportional navigation has been very popular both in theoretical research and practical applications. It is most extensively used in short range guidance. It follows from the fact that when the direct

line-of-sight between two vehicles does not change direction as the range closes, they are on a collision course. The first application of proportional navigation in modern missile systems can be dated back to the 1940s. Since that time, proportional navigation has become the most often utilised empirical guidance law, because of its efficiency, simplicity and simplicity of execution. It also has attracted a significant amount of interest in the literature. The PNG law, in theory, provides acceleration commands that are proportional to the closing velocity and LOS rate. Mathematically, it can be expressed as

$$a_{MC} = NV_c\dot{\hat{q}} \tag{4.1}$$

where a_{MC} is the acceleration instruction, N is a dimensionless gain selected by the designer (typically 3-5) termed as the effective navigation ratio, V_c denotes the closing velocity of the missile and $\hat{q}$ is the estimated LOS angle.

4.3 Noise Filter and Flight Control

It is critical from the standpoint of guidance to keep the intercept time and distance between the missile and the target as short as possible (ideally zero). The closest distance between the target and the missile when it hits is called the miss distance. The missile seeker's major goal is to calculate the LOS rate as accurately as possible so that the proportional navigation guiding law may be established. However, noise is a significant factor in determining the LOS rate. The noise present within the radar and the signals brings down the accuracy in measurement and thus, significantly affects the miss distance. Noise is a concern in radar and infrared systems as it affects the miss distance considerably. The primary impact of noise is to obscure the true LOS rate. Noise is introduced in the system due to missile receiver effects or target effects. Thermal noise created by the antenna and receiver circuitry accounts for the majority of receiver noise. It is produced in the receptor of the missile, and must compete with the target signal. Otherwise, it

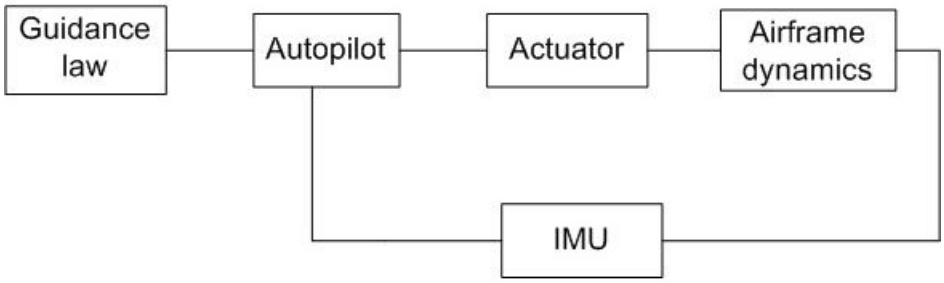

Figure 4.3: Basic elements of missile flight control system

may result in lowest SNR. As a result, a digital noise filter is required to obtain the LOS rate estimate $\hat{\dot{q}}$ required by the PN guidance.

The flight control system takes a crucial role in the functionality of the guidance loop. Figure 1 depicts the essential components of a flight control system. 4.3. It consists of a feedback control loop. An inertial measurement unit (IMU) functions as a feedback elements which measures the missile's angular velocity and translational acceleration. In majority of flight control operations, IMU is made up of gyroscopes and accelerometers to calculate three components of missile's linear acceleration and three components of its angular velocity. It is commonly represented as a second order transfer function for early design and analysis. The IMU's outputs are combined with the guiding instruction to form the specified control command, such as a required thrust-vector angle or tail-surface deviation which is fed to the actuator. The autopilot needs to be designed such that the control command does not create oversaturation problem in the actuator or the IMU. In most cases, the actuator is an electromechanical system that observes the physical control signal in order to go after the ordered control command. The airframe kinetics follows the control signal and creates the measurable quantities by the IMU. The kinetics of the airframe is regulated by the Newtonian laws of motion. The missile's aerodynamic behavior, thrust, and mass attributes dictate the features of the airframe dynamics. The main objective of the flight control system is to track the guidance commands and compel the missile dynamics to

follow them in a well defined manner.

According to Nesline and Zarchan[52], the transfer function used to represent the system behavior from the LOS rate ($\dot{q}_s$) to missile acceleration a_M is given by

$$\frac{a_M}{\dot{q}_s}(s) = \frac{NV_c}{(1+\frac{sT_G}{n})^n}, \tag{4.2}$$

where T_G is the time constant of the guidance system and n irepresents the order of the system. Taking the system order $n = 4$,

$$\frac{a_M}{\dot{q}_s}(s) = \frac{NV_c}{(1+\frac{sT_G}{n})^4}. \tag{4.3}$$

4.4 Aerodynamic Transfer Function

The transfer function from commanded acceleration (from the guidance law) to missile body rate ($\dot{\nu}$) is approximated by the following aerodynamic transfer function:

$$\frac{\dot{\nu}}{a_M}(s) = \frac{1+sT_\alpha}{V_m}, \tag{4.4}$$

where T_α represents the turning rate time constant and V_m denotes the speed of the missile.

4.5 Effect of Radome Error on Guidance Loop

A radar antenna is protected by a radome, which is a waterproof structure. In case of homing missiles, the radome is protects the seeker antenna from thermo-mechanical stresses. But the radar signal gets refracted when it goes

through the radome. This phenomenon results in erroneous LOS rate. This is termed as the radome error. Radome error forms a parasitic loop inside the guidance system, affecting the miss distance and even disrupting the guidance loop's stability. Let us now mathematically analyse the effect of radome error in guidance performance.

Figure 4.4 illustrates the principles of radome refraction. Because the radome refracts the radar signal, the target seems to be moved from its actual position. The angular difference between the two is known as the radome refraction angle (η). It depends on the gimbal angle θ_B of the seeker.

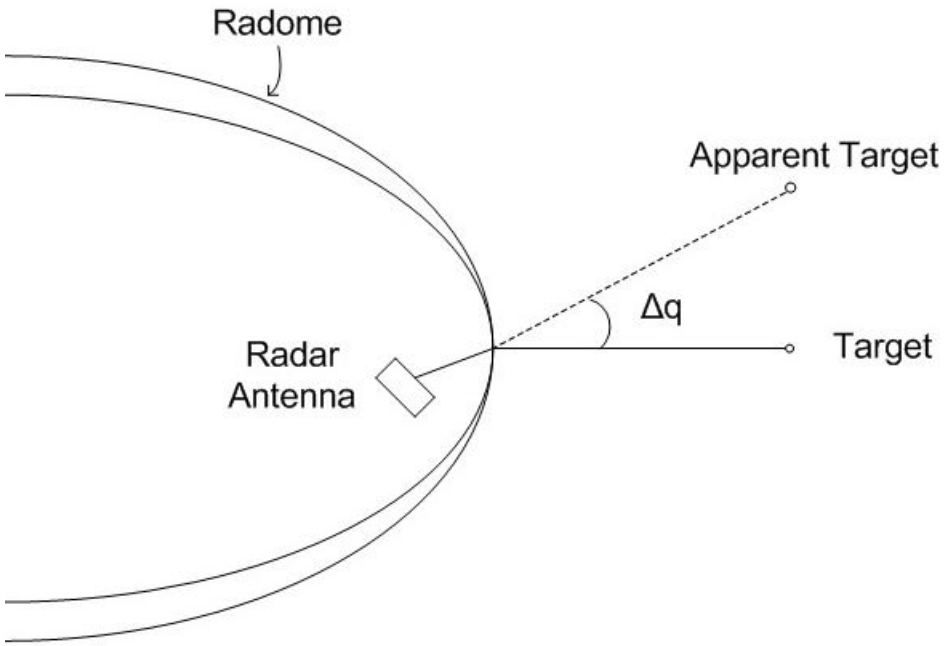

Figure 4.4: Radome refraction physics

The radome error slope is given as the rate of variation of the radome refraction angle in relation to the gimbal angle and is expressed as

$$R = \frac{d\eta}{d\theta_B}. \tag{4.5}$$

Considering R to be fixed, the radome refraction angle changes linearly with the seeker gimbal angle. It is given as

$$\eta = R\theta_B. \tag{4.6}$$

The basic missile-target geometry has already been shown in Fig. 4.2. From the geometry, the true LOS angle is represented as

$$q_t = q^* - \Delta q, \tag{4.7}$$

where q_t is the true LOS angle, q^* is the apparent LOS angle and Δq is the radome refraction angle which was previously denoted as η. Using the result from equation (3.6) in equation (3.7), we get

$$\begin{aligned} q_t &= q^* - R\theta_B \\ &= q^* - R(q_s - \nu), \end{aligned}$$

where q_s represents the seeker dish angle, ν represents the body attitude angle and the result $\theta_B = q_s - \nu$ follows from the missile-target geometry. Rearranging the above equation, we arrive at

$$q^* = q_t + R(q_s - \nu). \tag{4.8}$$

The tracking error angle ε can now be ignored in a steady tracking scenario. Hence it follows that $q_s \approx q_t$. So, equation (3.8) is written as

$$q^* = q_t + R(q_- v)$$
$$= q_t(1+R) - Rv.$$

In practical conditions, radome error slope iswell below unity ($R \ll 1$). Hence, we arrive at

$$q^* = q_t - Rv. \tag{4.9}$$

Equation (3.9) will be incorporated in the detailed seeker block diagram later on.

4.6 Effect of Beam Pointing Error on Guidance Loop

Phased array antennas find extensive application in missile seekers. A phased array antenna is an array antenna in which a single radiator can be fed with different phase shifters. It is based on the principle of electronic steering, in which the beam of radio waves can be steered in multiple directions without physically moving the antenna. Electronic steering is much more flexible and efficient than mechanical steering and also requires less maintenance. The principle of phased array antenna is based on interference, i.e., phase-dependent superposition of two or more radiation sources.

Figure 4.5 shows the arrangement of phase shifters in case of phased array radar antenna. The radiating elements are situated at a distance d apart from each other. θ_B is known as the beam steering angle or simply the beam angle. x represents the path difference between successive elements and $\Delta\phi$ represents the phase shift between two successive elements. From the right angled triangle,

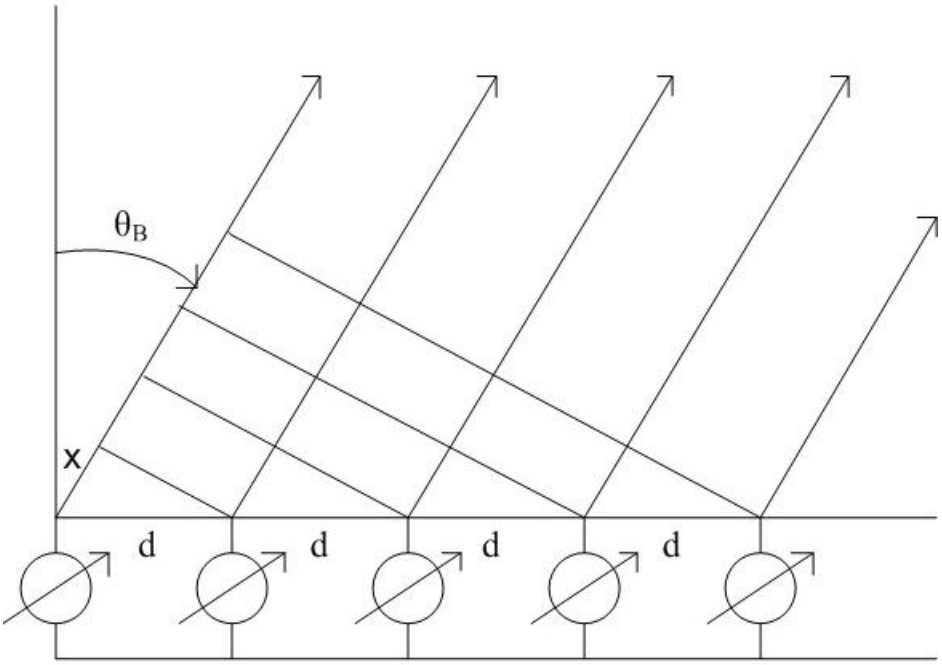

Figure 4.5: Phased array antenna

$$\sin\theta_B = \frac{x}{d}$$

$$\text{or,} \quad x = d\sin\theta_B.$$

Now, we know that the relationship between phase difference and path difference can be expressed as

$$\Delta\phi = \frac{2\pi}{\lambda}d.$$

Combining the above results, we can write

$$\Delta\phi = \frac{2\pi}{\lambda}\sin\theta_B. \tag{4.10}$$

Hence, the gimbal angle θ_B can be computed as

$$\theta_B = sin^{-1}(\frac{\lambda}{2\pi d}\Delta\phi_B). \tag{4.11}$$

The beam command diagram is shown in Fig. 4.6. The beam angle control command is denoted by θ_{BC}. First, ideal phase is calculated using the control command as

$$\Delta\theta_B^* = \frac{2\pi d}{\lambda}\sin\theta_{BC}. \tag{4.12}$$

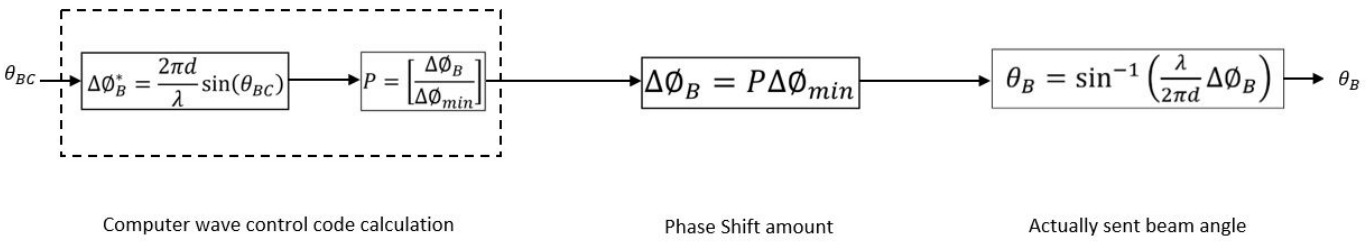

Figure 4.6: Antenna beam control
[53]

Now the digital phase shifter provides the phase shift, which is displayed in binary digits. For a K-bit phase shifter, the minimal $\Delta\phi$ is

$$\Delta\phi_{Bmin} = \frac{2\pi}{2^K}. \tag{4.13}$$

The purpose of the digital phase shifter is to perform quantization. The beam control code represents the number of each beam, $P = 0, 1, 2, ..., 2^k - 1$ and is given by

$$P = \frac{\Delta\theta_B^*}{\Delta\phi_{Bmin}}. \tag{4.14}$$

As a result of this quantization, the real beam angle provided by the phase shifter is not identical to the control input θ_{BC}. The true phase provided by the phase shifter is obtained as

$$\Delta\theta_B = P\Delta\phi_{min}. \tag{4.15}$$

Hence, the real beam angle is obtained as

$$\theta_B = sin^{-1}(\frac{\lambda}{2\pi d})\Delta\phi_B. \tag{4.16}$$

The beam pointing error slope is interpreted as the rate of fluctuation of the error between the beam control command (θ_{BC}) and the real beam angle θ_B with respect to the beam control command. It is mathematically expressed as

$$R^* = \frac{\delta\Delta\theta}{\delta\theta_{BC}}. \tag{4.17}$$

where R^* is the beam pointing error slope and $\Delta\theta = \theta_{BC} - \theta_B$.
For small time variations,

$$\Delta\theta_{BC} = \theta_{BC} - \theta_B = R^*\theta_{BC}$$
$$\text{or,} \quad \theta_B = (1 - R^*)\theta_{BC}.$$

The target tracking control loop diagram of Phased Array Radio Seeker (PARS) incorporating the beam pointing control is given in Fig.4.7. The important notations corresponding to the control loop is shown in the table below.

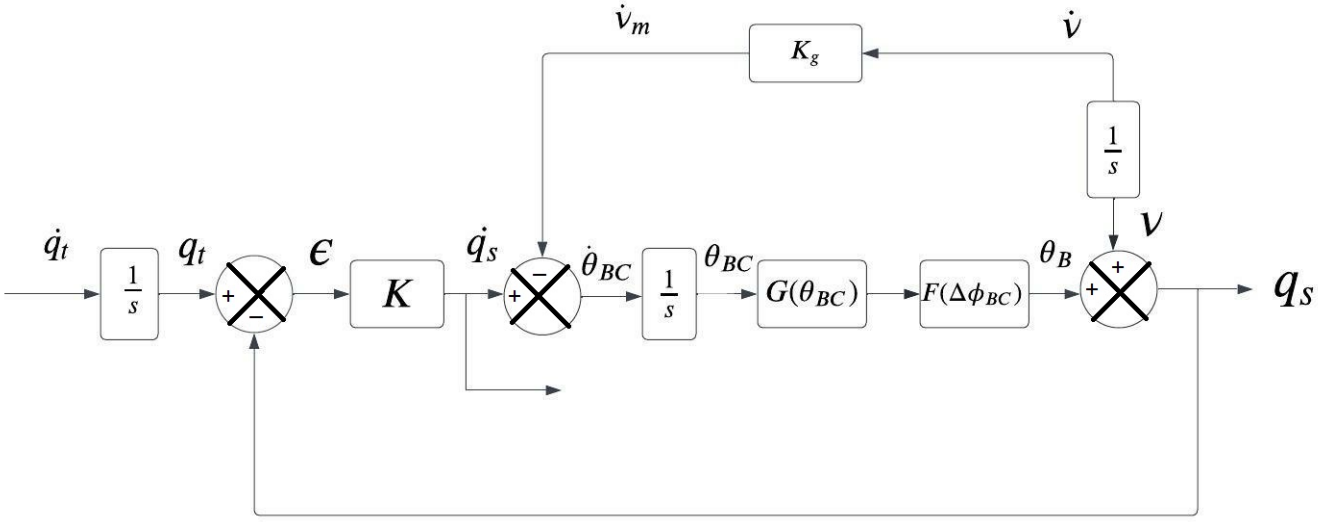

Figure 4.7: Beam control loop of PARS

K	The seeker forward loop gain
$\dot{\nu}_m$	Angular speed of the body measured by IMU
K_g	Angular rate gyro scale
$F(\Delta\phi_{BC})$	Beam control unit
$G(\theta_{BC})$	Beam control unit
$\Delta\phi_{BC}$	Reading element phase shift value

According to the control loop, the beam angle control command (θ_{BC}) and the actual beam angle θ_B are related via the beam control units as

$$\theta_B = F(\Delta\phi_{BC})G(\theta_B). \tag{4.18}$$

According to the results derived above, the control unit can be represented in terms of the beam pointing error slope as

$$F(\Delta\phi_{BC})G(\theta_B) = 1 + R^*. \tag{4.19}$$

4.7 Block Diagram and Transfer Function of Seeker With DRE Parasitic Loops

The effect of disturbance inputs is to create two parasitic loops inside the guidance loop discussed in Fig. 4.1. The parasitic loops affect the coupling of the measurements with the movement of the body of the missile and thus results in performance degradation and increased miss distance.

These two loops are combined together to form a single loop termed as the DRE parasitic loop. Fig. 4.8 depicts a schematic diagram of the DRE parasitic loop. The schematic representation of the guidance loop after incorporation of the DRE parasitic loop is depicted in Fig. 4.9. The block diagrams are derived with a simple assumption that the missile high - accuracy inertial system's angular rate gyro gauge Kg has a narrow variation band. and $K_g \approx 1$.

Now let us analyse the block diagram in a bit more detail. Truly speaking, the missile body motion can influence the LOS angular rate. Analyzing Fig.4.9, LOS rate $\dot{q}_s$ is expressed as

$$\begin{aligned}\dot{q}_s &= \frac{Kq_t - K\dot{v}R + \dot{K}(+R^*)\dot{v} - K\dot{v}}{s + K(1+R^*)} \\ &= \dot{q}_t\left(\frac{K}{s+K(1+R^*)}\right) + \dot{v}\left(\frac{K(1+R^*) - KR - K}{s+K(1+R^*)}\right).\end{aligned}$$

The element produced by the motion of the body is given by

$$\Delta\dot{q}_s = \dot{v}\left(\frac{K(1+R^*) - KR - K}{s+K(1+R^*)}\right). \tag{4.20}$$

Hence we can write

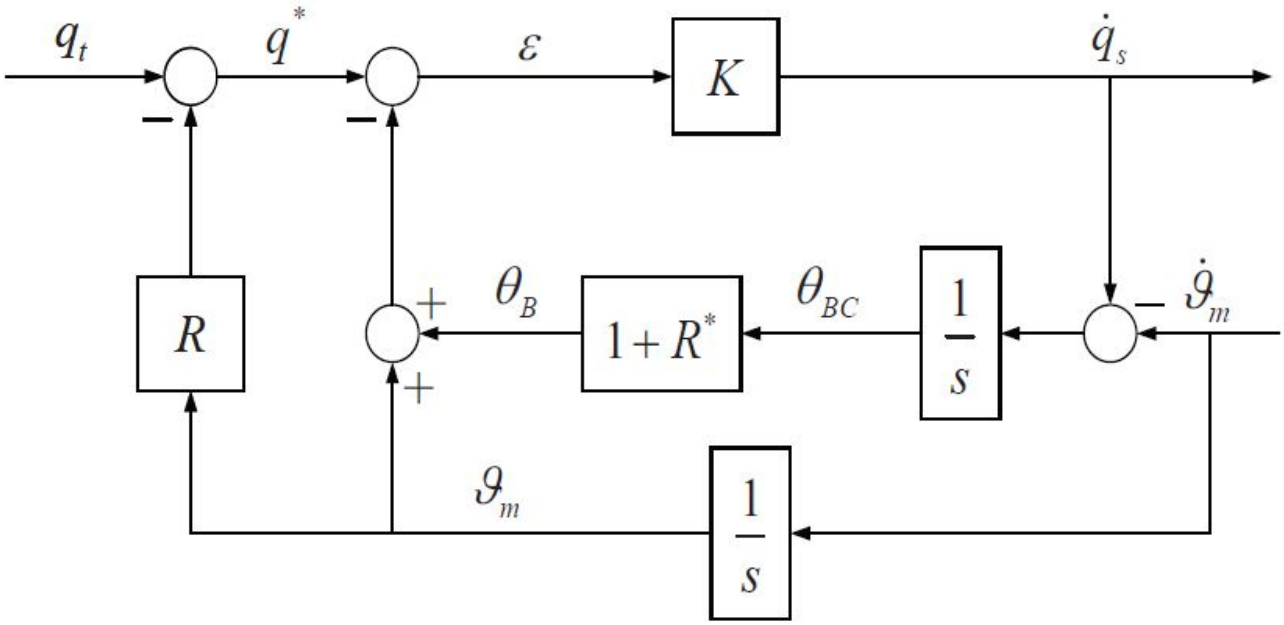

Figure 4.8: The schematic representation of DRE parasitic loop
[1]

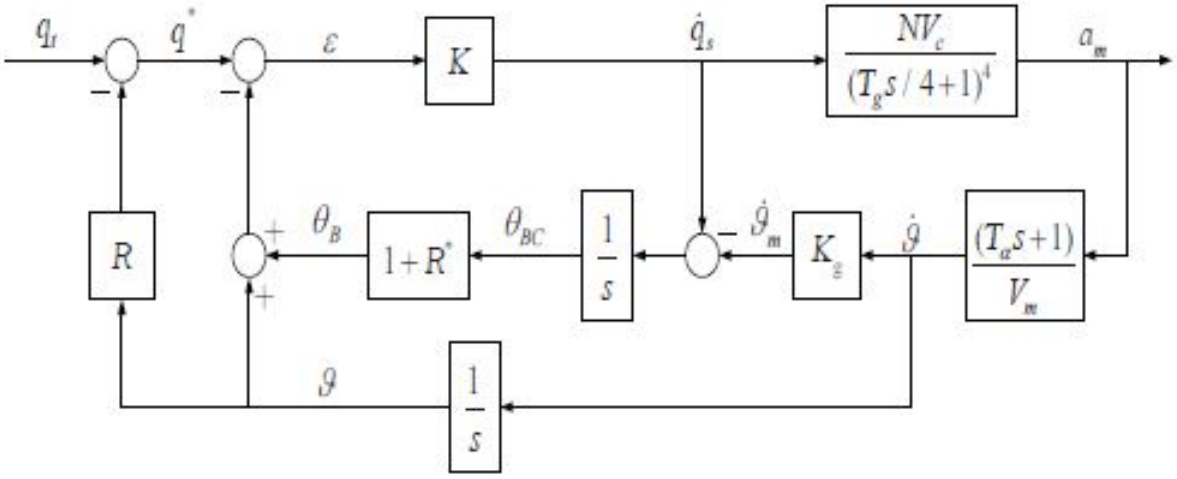

Figure 4.9: The schematic representation of guidance loop with DRE parasitic loop
[1]

$$\frac{\Delta \dot{q}_s}{\dot{v}} = \frac{R^* - R}{\frac{s}{K} + R^* + 1}. \tag{4.21}$$

Hence, the DRE function is expressed as

$$G_{DRE} = \frac{R^* - R}{\frac{s}{K} + R^* + 1}. \tag{4.22}$$

Thus it is clear that R and R^* both constitute the DRE problem. From Fig.4.9, the closed loop transfer function from true LOS rate $\dot{q}_t$ to the missile acceleration a_M is represented as

$$\frac{a_M}{\dot{q}_t} = \frac{NV_c}{(\frac{s}{K} + 1 + R^*)\left(\frac{T_g}{4}s + 1\right)^4 + (R^* - R)\frac{NV_c}{V_m}(T_\alpha s + 1)}, \tag{4.23}$$

and thus the characteristic polynomial becomes

$$\Phi(s) = (\frac{s}{K} + 1 + R^*)\left(\frac{T_g}{4}s + 1\right)^4 + (R^* - R)\frac{NV_c}{V_m}(T_\alpha s + 1). \tag{4.24}$$

Both radome error and beam directing error certainly have an impact on the stability region. Using Routh Stability Criterion, it can be shown that The greater the magnitude of the total error gradient $R^* - R$, the lesser stable it is [1]. The detailed derivation is not shown in this work as it will greatly shift our objective. However, clearly the existence of the parasitic loops has important role on the stability and precision of the missile guidance, which can result in larger miss distance.

Chapter 5

Estimation of Seeker Signals Using ESKF

5.1 Problem Statement

In this chapter, the problem associated with the radome error and the beam pointing error, or in short, the DRE problem will be addressed and the LOS data will be estimated using the ESKF. The ESKF algorithm has already been discussed in Chapter 3. The LOS angle q_t, angular rate $\dot{q}_t$ and the seeker gimbal angle θ_B are taken as the three state variables of the system. The radome and the beam pointing error slopes R and R^* are taken as the slowly varying uncertain dynamics of the system and hence, the two extended states of the system according to the ESKF algorithm. The radome error slope predicted value $\hat{R}$, the beam pointing error slope predicted value $\hat{R}^*$, the true LOS angle prediction $\hat{q}_t$ and the estimate of actual LOS rate, $\hat{\dot{q}}_t$ can be effectively computed from the filter. As a result, the DRE parasitic loop's online prediction and correction is accomplished. The system state variables and the extended states are set as

$$X = [X_1 \quad X_2 \quad X_3]^T = [q_t \quad \dot{q}_t \quad \theta_B]^T, \tag{5.1}$$

$$F = [X_4 \quad X_5]^T = [R \quad \dot{R}]^T. \tag{5.2}$$

The measured output is taken from the LOS angular rate $\dot{q}_s$ and is calculated by

$$Z = \dot{q}_s. \tag{5.3}$$

After substituting the real variables with the notation of phase variables, Fig. 4.8 can be redrawn as Fig. 5.1. According to Fig. 5.1, the state space representation of the system can be expressed as

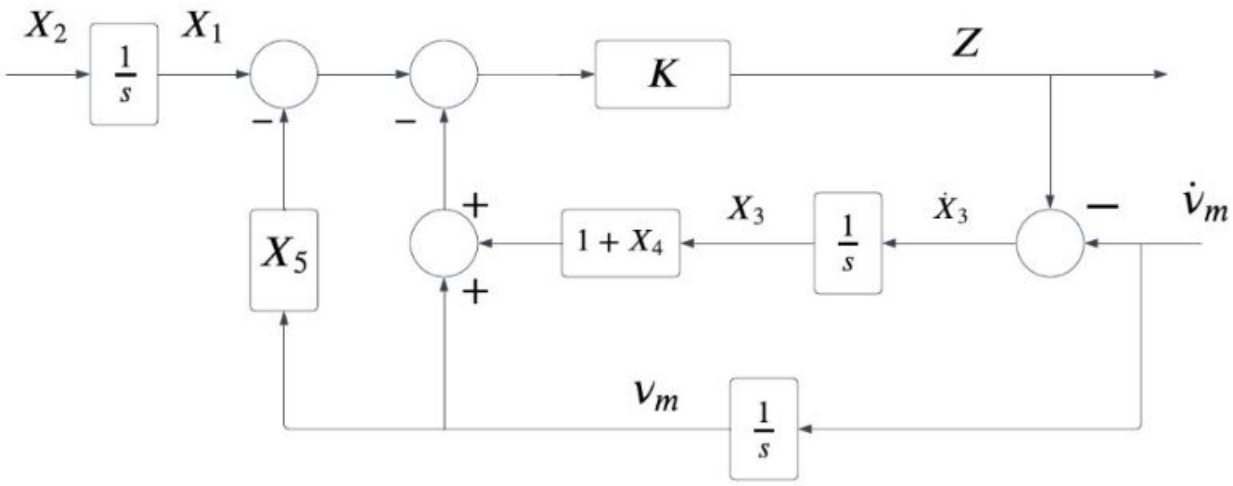

Figure 5.1: Phase variable representation of DRE parasitic loop

$$\begin{bmatrix} \dot{X}_1 \\ \dot{X}_2 \\ \dot{X}_3 \end{bmatrix} = \begin{bmatrix} 0 & 1 & 0 \\ 0 & 0 & 0 \\ K & 0 & -K \end{bmatrix} \begin{bmatrix} X_1 \\ X_2 \\ X_3 \end{bmatrix} + \begin{bmatrix} 0 & 0 \\ 0 & 0 \\ -KX_3 & -Kv_m \end{bmatrix} \begin{bmatrix} X_4 \\ X_5 \end{bmatrix} + w(t), \tag{5.4}$$

where $w(t)$ represents the vector representing the process noise given by $w(t) = [w_1(t) \quad w_2(t) \quad w_3(t)]^T$. The output is expressed as

$$Z = \begin{bmatrix} K & 0 & -K & -KX_3 & -Kv_m \end{bmatrix} \begin{bmatrix} X \\ F \end{bmatrix} + v(t). \tag{5.5}$$

Here $v(t)$ denotes the noise in the measurement system and

$$X = [X_1 \quad X_2 \quad X_3]^T, \qquad F = [R^* \quad R]^T.$$

F represents the nonlinear uncertain dynamics of the system according to the ESKF design process discussed in Chapter 3. Now, the state and measurement equations are discretized using the sample time Δt. Hence, the discrete fundamental matrix $\tilde{A}_k$ and the discrete disturbance matrix $\tilde{B}_k$ are obtained as

$$\tilde{A}_k = \begin{bmatrix} 1 & \Delta t & 0 \\ 0 & 1 & 0 \\ K\Delta t & 0 & 1-K\Delta t \end{bmatrix}, \tag{5.6}$$

$$\tilde{B}_k = \begin{bmatrix} 0 & 0 \\ 0 & 0 \\ -KX_3\Delta t & -K\nu_m\Delta t \end{bmatrix}. \tag{5.7}$$

In accordance with the ESKF methodology, the discrete extended state matrices A_k, B_k and C_k can then be expressed as

$$A_k = \begin{bmatrix} 1 & \Delta t & 0 & 0 & 0 \\ 0 & 1 & 0 & 0 & 0 \\ K\Delta t & 0 & 1-K\Delta t & -KX_3\Delta t & -K\nu_m\Delta t \\ 0 & 0 & 0 & 1 & 0 \\ 0 & 0 & 0 & 0 & 1 \end{bmatrix}, \tag{5.8}$$

$$B_k = \begin{bmatrix} 0 & 0 \\ 0 & 0 \\ -KX_3\Delta t & -K\nu_m\Delta t \\ 1 & 0 \\ 0 & 1 \end{bmatrix}, \tag{5.9}$$

$$C_k = \begin{bmatrix} K & 0 & -K & -KX_3 & -K\nu_m \end{bmatrix}. \tag{5.10}$$

The process noise power spectral densities are designed as S_{w1}, S_{w2} and S_{w3} and the discrete system noise covariance matrix is thus given as

$$S_k = \begin{bmatrix} \frac{S_{w1}}{\Delta t} & 0 & 0 \\ 0 & \frac{S_{w2}}{\Delta t} & 0 \\ 0 & 0 & \frac{S_{w3}}{\Delta t} \end{bmatrix}. \tag{5.11}$$

The unspecified disturbance matrix H_k is given by

$$H_k = F_k - F_{k-1} = \begin{bmatrix} R_k^* + w_4(k) - R_{k-1}^* - w_4(k-1) \\ R_k + w_5(k) - R_{k-1} - w_5(k-1) \end{bmatrix}. \tag{5.12}$$

The ESKF is used to predict and correct the unpredictable disruption. Thus, the estimate of the unknown disturbance matrix is given as

$$\hat{H}_k = \hat{F}_k - \hat{F}_{k-1} = \begin{bmatrix} \hat{R}_k^* - \hat{R}_{k-1}^* \\ \hat{R}_k - \hat{R}_{k-1} \end{bmatrix}. \tag{5.13}$$

The extended model disturbance estimation covariance matrices $Q_{1,k}$ and $Q_{2,k}$ is given by

$$Q_{1,k} = \begin{bmatrix} 0_{3x3} & 0_{3x2} \\ 0_{2x3} & 4\bar{Q} \end{bmatrix}, \tag{5.14}$$

where

$$\bar{Q} = 2 \begin{bmatrix} \hat{R}_k^* - \hat{R}_{k-1}^* & 0 \\ 0 & \hat{R}_k - \hat{R}_{k-1} \end{bmatrix}, \tag{5.15}$$

$$Q_{2,k} = \begin{bmatrix} S & 0_{3x2} \\ 0_{2x3} & 0_{2x2} \end{bmatrix}. \tag{5.16}$$

The discrete noise driven covariance matrix Γ_k is designed as

$$\Gamma_k = \Delta t . I_{5x5}, \tag{5.17}$$

where I represents the identity matrix. The enhanced model's measurement noise covariance matrix is now designed as follows:

$$R_k = \sigma_v^2. \tag{5.18}$$

Thus, the design of the ESKF for the real-time prediction and correction for the DRE loop is as follows

$$K_k = -A_k P_k C_k^T \left(C_k P_k C_k^T + \frac{1}{\Delta t + \theta} R_k \right)^{-1}, \tag{5.19}$$

$$P_{k+1} = (\Delta t + \theta)(A_k + K_k C_k) P_k (A_k + K_k C_k)^T + K_k R_k K_k^T + \left(1 + \frac{1}{\theta} \right) Q_{1,k} + \Gamma_k Q_{2,k} \Gamma_k^T \Big). \tag{5.20}$$

5.2 Simulation Results and Discussions

The ESKF approach is utilised for the online prediction and compensation of the parasitic loop produced by the disturbance inputs, as described in the preceding section. MATLAB simulations are performed to correctly estimate and compensate the radome error slope R, beam pointing error slope R^* and thus, estimation of the actual LOS data is performed. The simulation conditions are given below.

$$\sigma_v = 0.2,$$
$$S_{w1} = 0.001,$$
$$S_{w2} = 0.001,$$
$$S_{w3} = 0.001.$$

The missile body movement is considered to be sinusoidal, with a magnitude of 3^o and a frequency of 2 Hz. It is also supposed that the disturbance inputs are originally varying sinusoidally as

$$R = 0.6 \sin \pi t,$$
$$R^* = 0.6 \cos \pi t.$$

The initial values of the state and uncertainty vectors are given as

$$X_0 = [0 \quad 0 \quad 0]^T,$$
$$F_0 = [0.6 \quad 0]^T.$$

The starting value of the extended model's error covariance matrix is considered as $P_0 = 0.1 I_{5x5}$. The initial estimation values of the ESKF has been randomised based on the true initial values. A Monte Carlo simulation has been performed over 100 runs. In each Monte Carlo run, the filter has been run for 5 seconds in steps of 0.01 seconds. Fig. 5.2 shows the prediction of the beam directing error gradient R^* for a specific run. The estimation of the radome error slope R for a specific run is depicted in Fig. 5.3. It may be observed that the ESKF estimates the slowly varying nonlinear disturbances quite accurately and then compensates

them. Therefore, the estimation of the true LOS angle q_t for that specific run is given in Fig. 5.4. Similarly, the estimation of the true LOS rate in that single run is given in Fig. 5.5.

Finally, the mean squared estimation error for LOS rate for 100 Monte Carlo runs has been shown in Fig. 5.6.

Next, a more powerful nonlinear disturbance was employed to demonstrate the effectiveness of ESKF. The disturbance inputs are described as

$$R^* = \begin{cases} 0.6\cos \pi t, & 0 \leq t < 1.5 \\ 0.8\sin 4\pi t, & 1.5 \leq t < 3.5 \\ 0.6\cos \pi t sign(\sin 2\pi t), & 3.5 \leq t < 5 \end{cases}$$

$$R = \begin{cases} 0.6\sin \pi t, & 0 \leq t < 1.5 \\ 0.8\cos 4\pi t, & 1.5 \leq t < 3.5 \\ 0.6\sin \pi t sign(\cos 2\pi t). & 3.5 \leq t < 5 \end{cases}$$

In the presence of the above nonlinearities, the ESKF has been run againwith the same parameter values. The estimation of the beam pointing error slope in this case has been shown in Fig. 5.7. Similarly, the estimation of the radome error slope has been shown in Fig. 5.8. The estimations of the true LOS angle and LOS rate have been depicted in Fig. 5.9 and Fig. 5.10 respectively. Finally, the mean squared estimation error for LOS rate for 100 runs in the case of stronger nonlinearities has been shown in Fig. 5.11.

From the above results, it can be said that the ESKF satisfactorily estimates the slowly varying nonlinear disturbance inputs even in case of stronger nonlinearities and then compensates them so that the filter can correctly estimate the important states of the system throughout the entire flight time, although, the MSE plot looked smoother in the previous case. In the next chapter, the performance of the ESKF will be compared to the EKF with the help of necessary simulations.

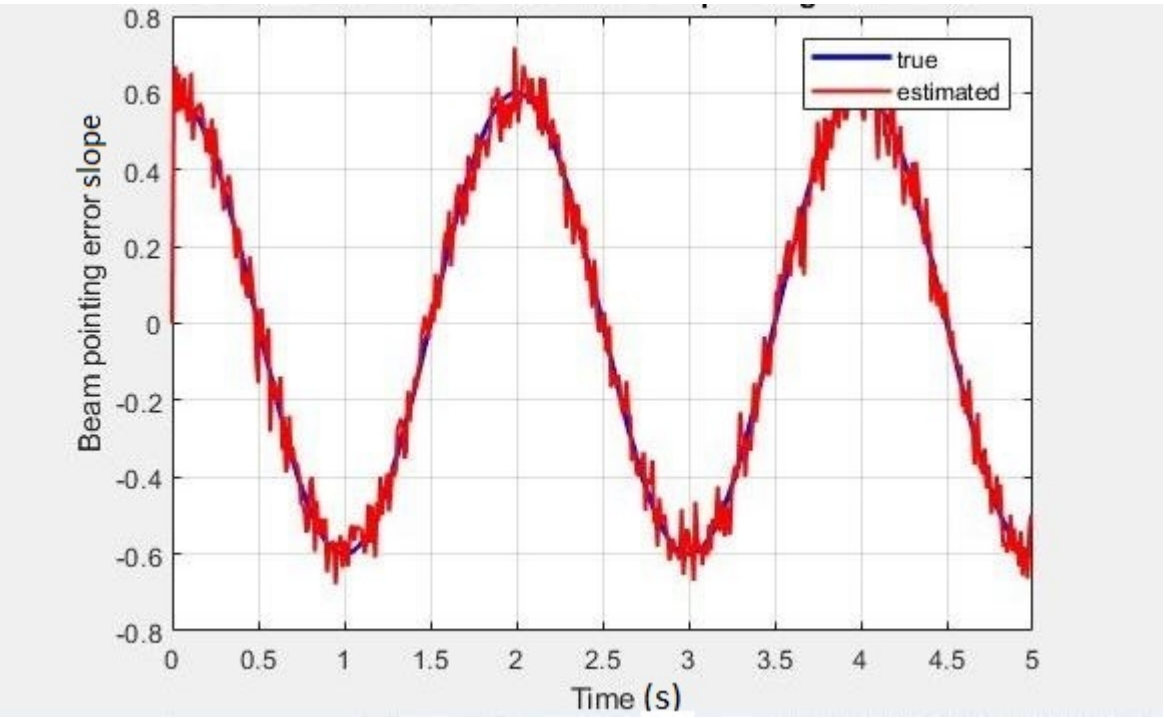

Figure 5.2: True and estimated state of beam pointing error slope for a particular run

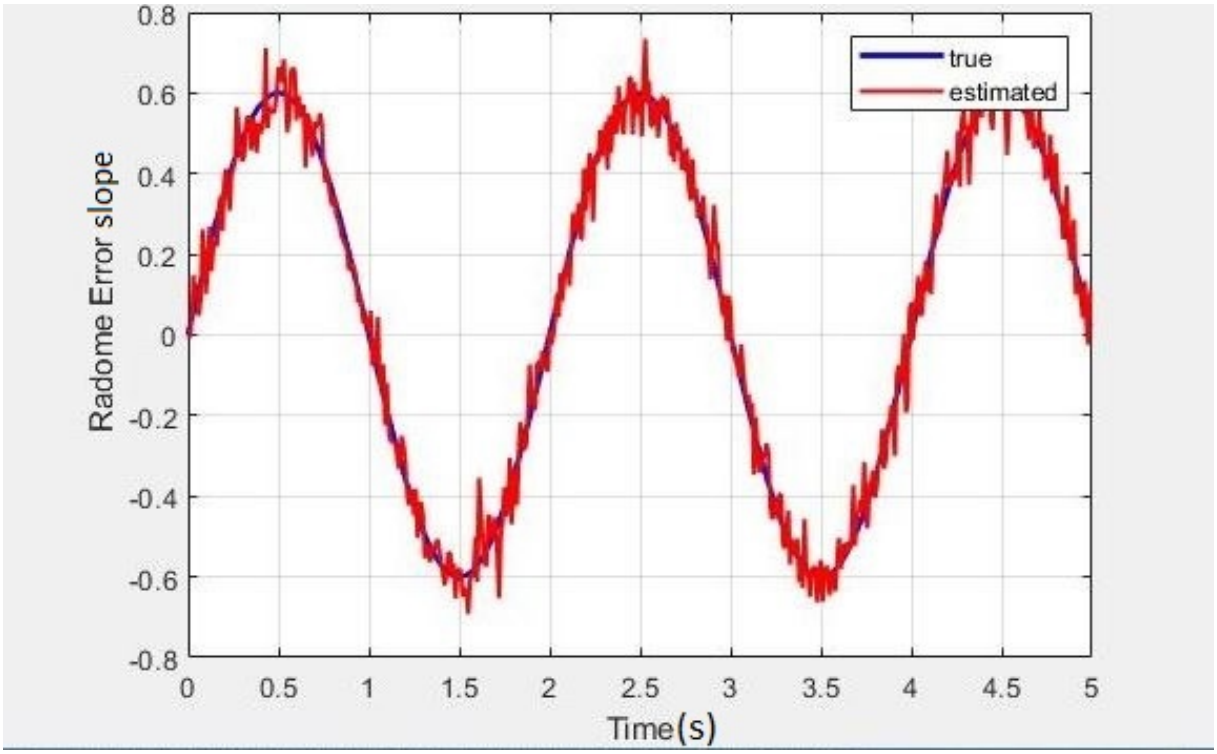

Figure 5.3: True and estimated state of radome error slope for a particular run

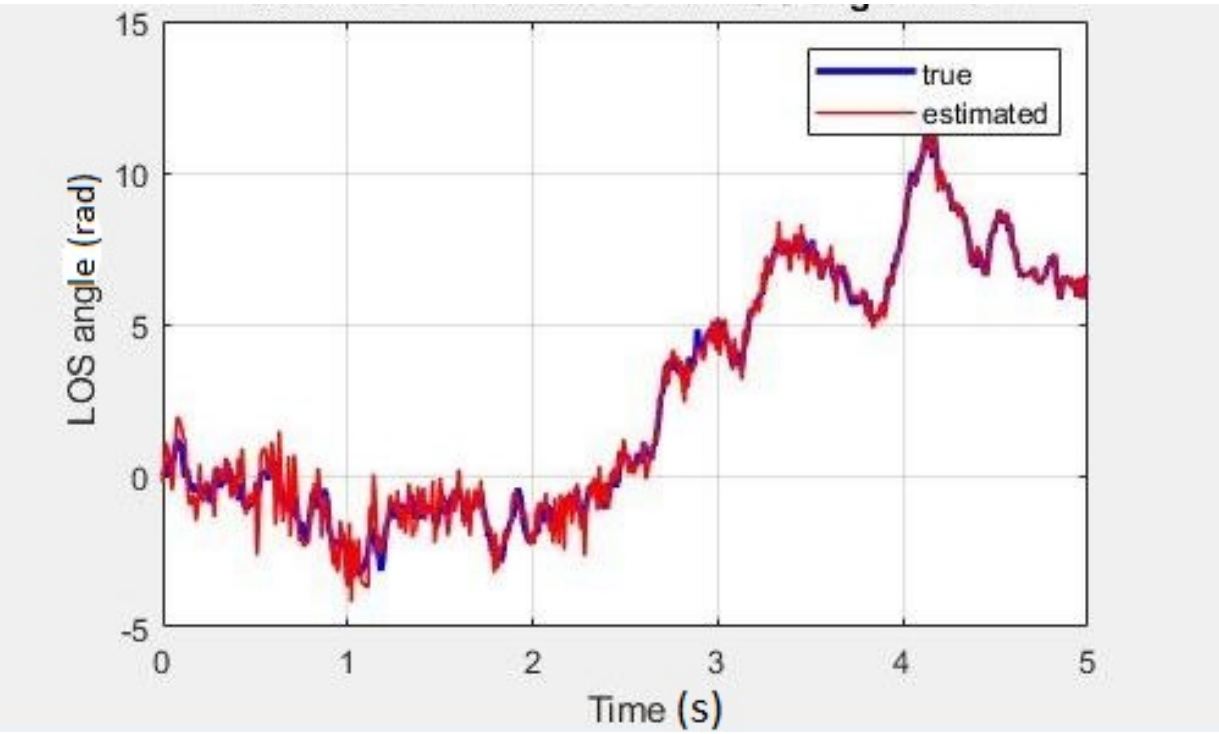

Figure 5.4: True and estimated state of LOS angle for a particular run

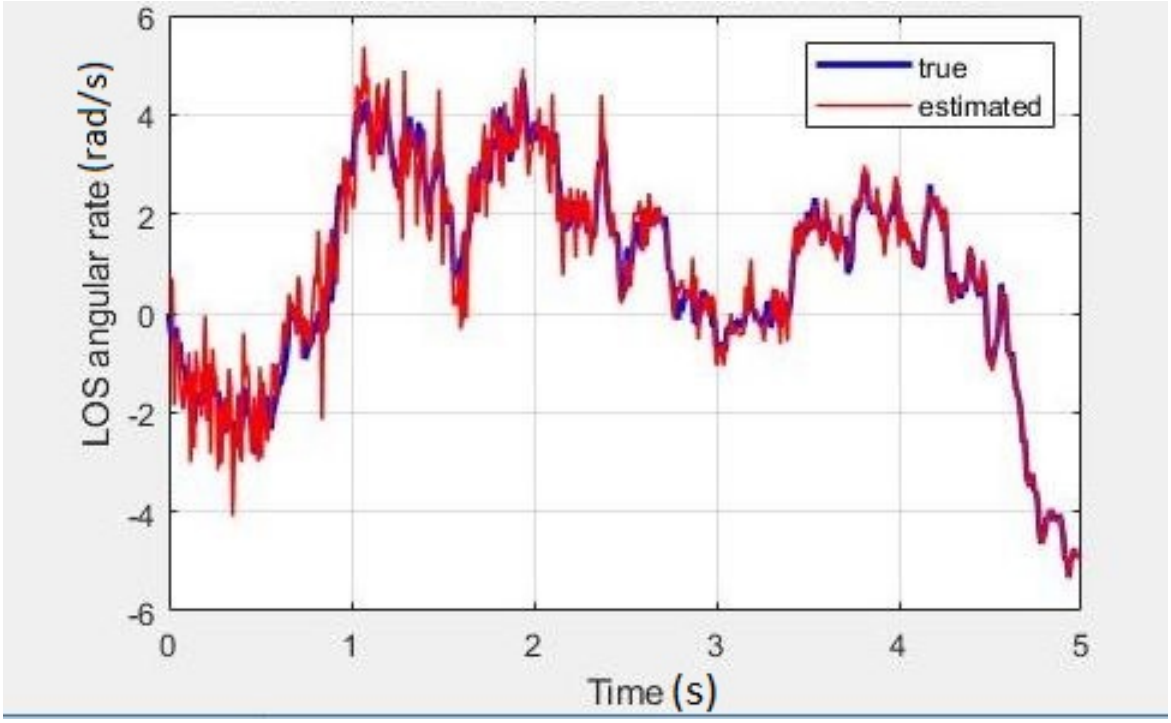

Figure 5.5: True and estimated state of LOS rate for a particular run

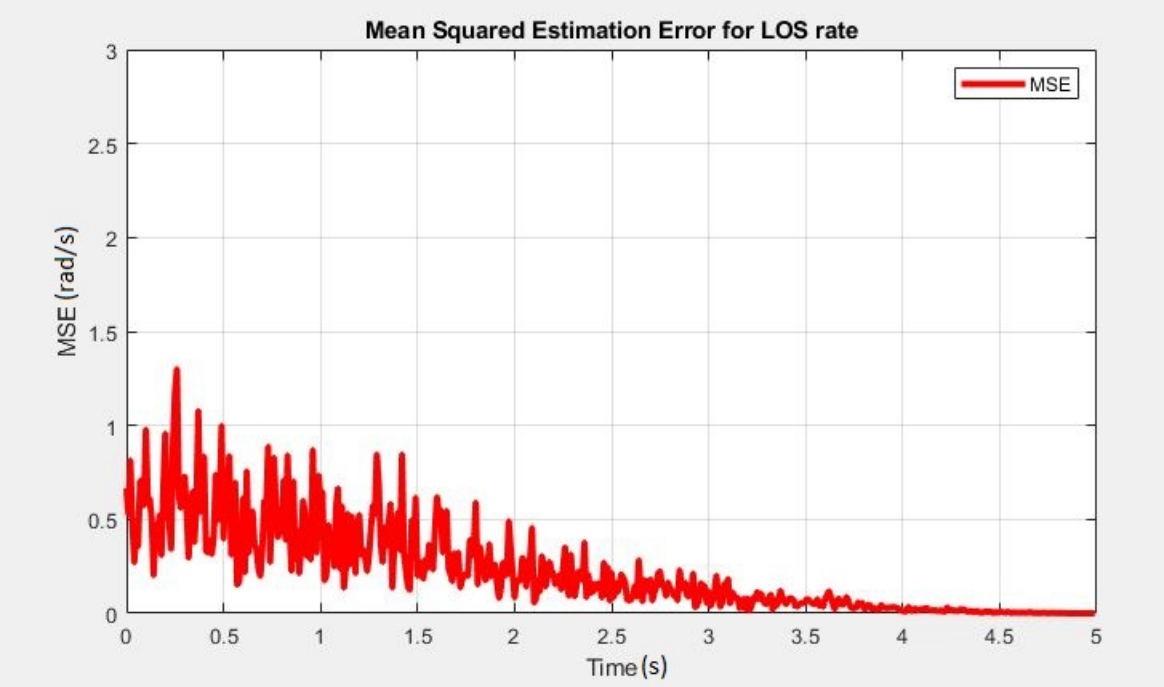

Figure 5.6: Mean squared estimation error for LOS rate

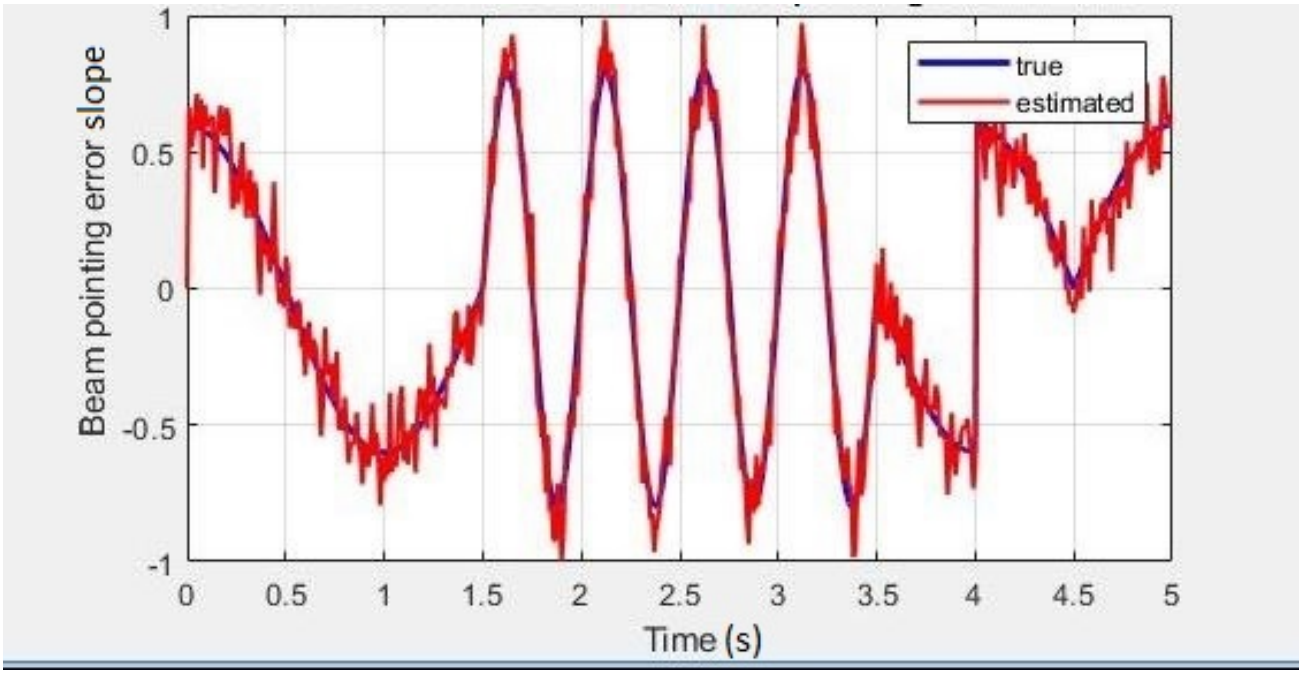

Figure 5.7: True and estimated state of beam pointing error slope for a particular run in case of stronger nonlinearity

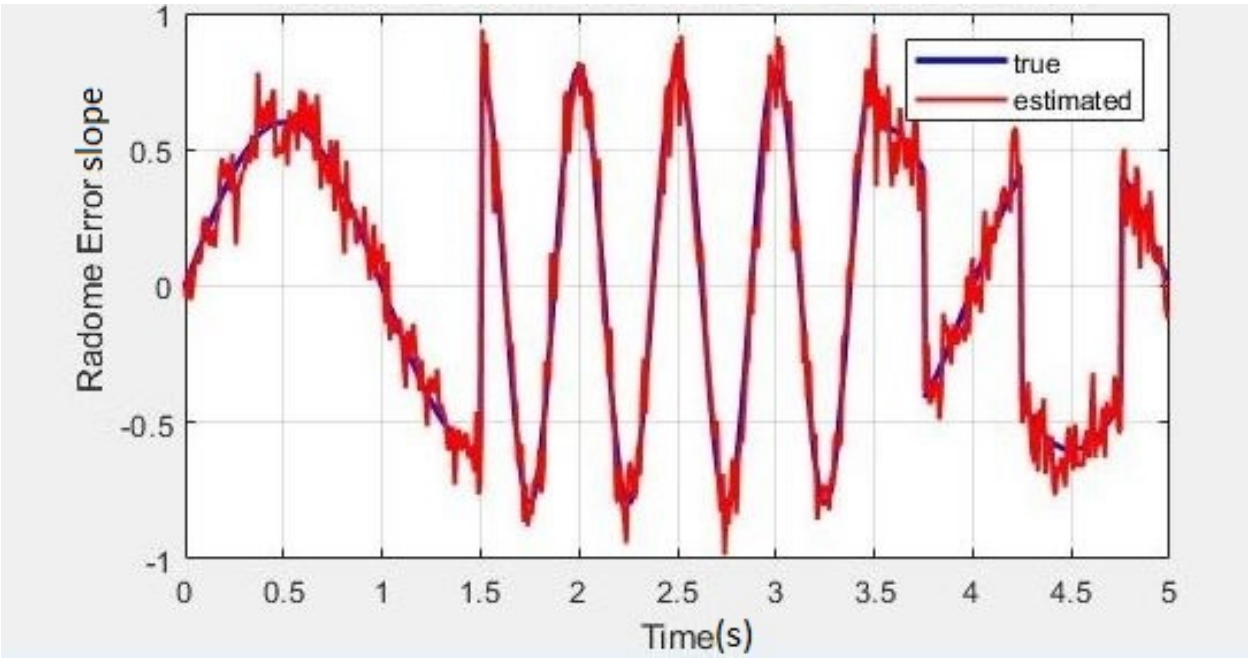

Figure 5.8: True and estimated state of radome error slope for a particular run in case of stronger nonlinearity

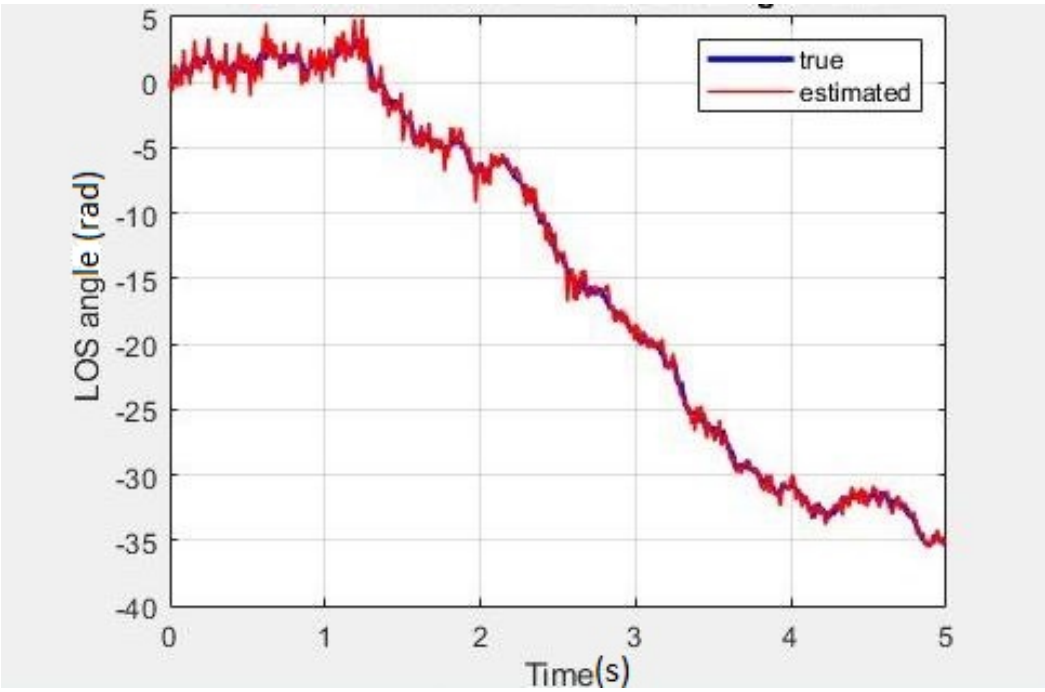

Figure 5.9: True and estimated state of LOS angle for a particular run in case of stronger nonlinearity

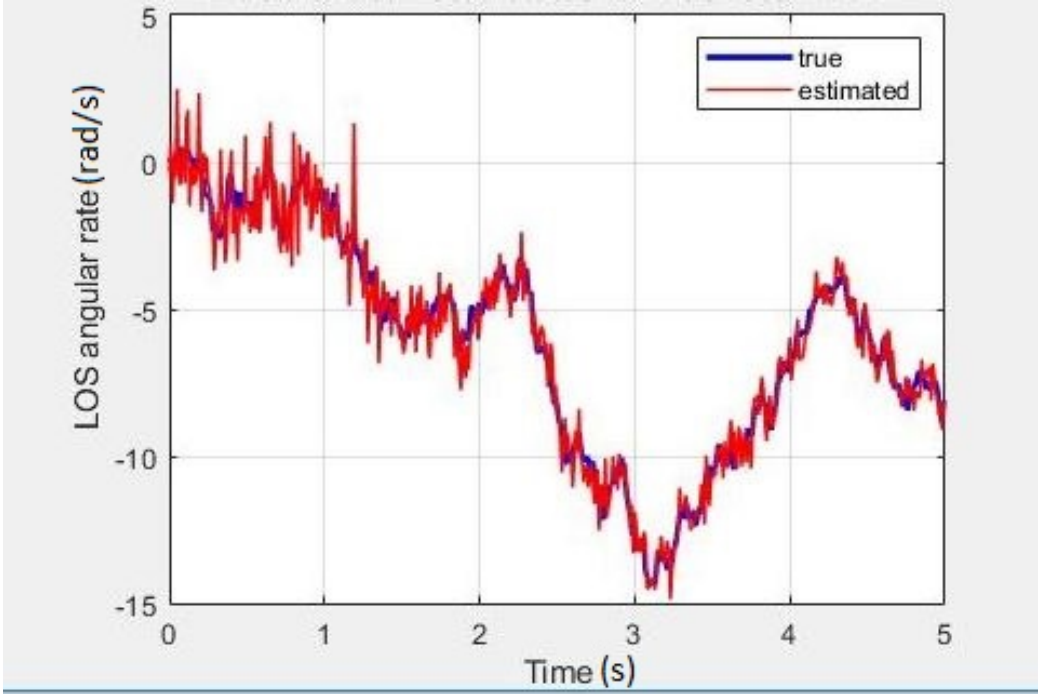

Figure 5.10: True and estimated state of LOS rate for a particular run in case of stronger nonlinearity

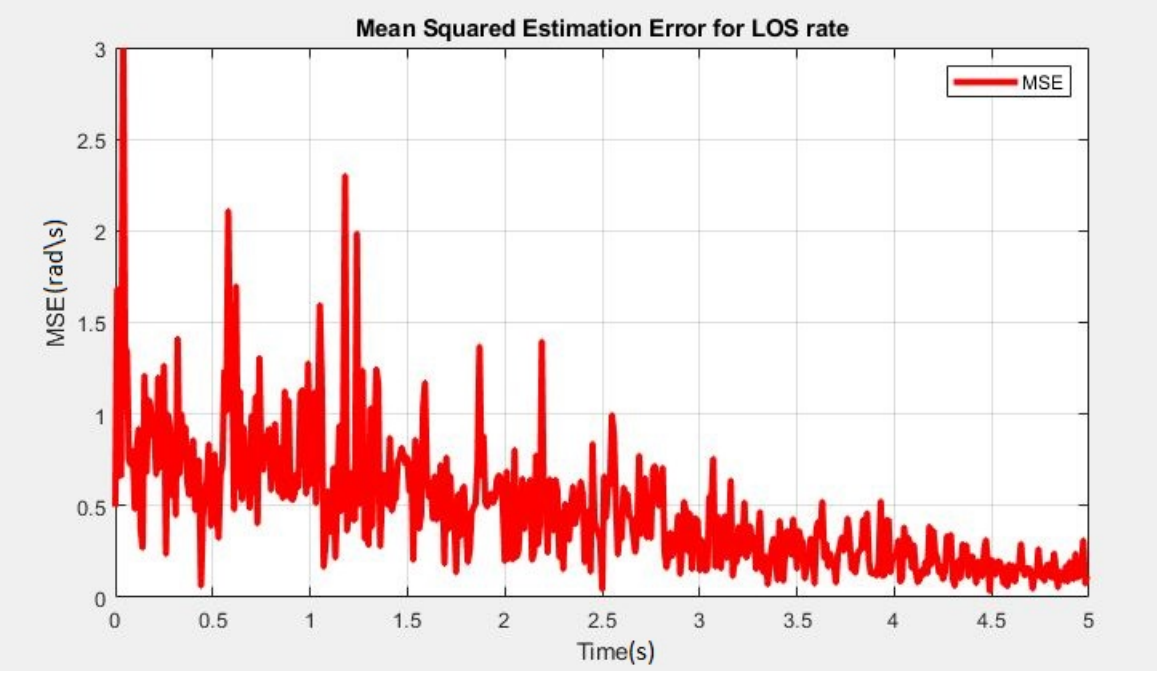

Figure 5.11: Mean squared estimation error for LOS rate in case of stronger nonlinearity

Chapter 6

Comparative Study of ESKF and EKF for Seeker Signal Estimation

6.1 The EKF-UI Algorithm

The Extended Kalman Filter (EKF) is a computing algorithm that solves the nonlinear estimation issue by linearizing the model about a prediction of the current mean and variance. The EKF has been extensively used for solving different engineering estimation problems including the missile guidance. For conventional EKF algorithm, the inputs are previously known and depending on the known inputs, the important states of the system are estimated. In many of the practical problems, it is necessary to predict the system states where the inputs to the system are non-deterministic or unknown. The estimation of seeker signals in the presence of parasitic loops discussed in the previous chapter is a prime example of such problem as both radome and beam pointing error slopes represent the unknown disruption inputs. In this chapter, the EKF problem in the presence of unknown inputs or the generalised EKF-UI algorithm has been briefly discussed, followed by necessary simulations to carry out the comparative study between ESKF and EKF-UI.

Consider the continuous time system represented by

$$\dot{x}_t = g(x, f, f^*, t) + w(t), \tag{6.1}$$
$$y(t) = h(x, f, f^*, t) + v(t), \tag{6.2}$$

where f and f^* represents the known and unknown inputs respectively. Compute the following linearized matrices

$$G_{k-1} = \left[\frac{\delta g}{\delta x}\right]_{\hat{x}_{k-1}, \hat{f}^*_{k-1}}, \tag{6.3}$$
$$B^*_{k-1} = \left[\frac{\delta g}{\delta f^*}\right]_{\hat{x}_{k-1}, \hat{f}^*_{k-1}}, \tag{6.4}$$
$$H_k = \left[\frac{\delta h}{\delta x}\right]_{\hat{x}_k, \hat{f}^*_{k-1}}, \tag{6.5}$$
$$D^*_k = \left[\frac{\delta g}{\delta f^*}\right]_{\hat{x}_k, \hat{f}^*_{k-1}}. \tag{6.6}$$

Hence, the EKF-UI algorithm can be given in brief as follows.

Step 0: Initialization

$$\text{Initialize} \quad x_0, f^*_0 \quad \text{and} \quad P_0$$

Step 1: Prediction

$$\hat{x}^-_k = \hat{x}^-_{k-1} + \Delta t\, g(\hat{x}_{k-1}, \hat{f}_{k-1}, \hat{f}^*_{k-1}).$$

Step 2: Gain Computation

$$\phi_{k-1} = I + \Delta t G_{k-1},$$

$$
\begin{aligned}
P_k^- &= \phi_{k-1} P_{k-1} \phi_{k-1}^T + Q_{k-1}, \\
K_k &= P_k^- H_k^T [H_k P_k^- H_k^T + R_k]^{-1}, \\
S_k &= [D_k^{*^T} R_k^{-1} (I - H_k K_k) D_k^*]^{-1}.
\end{aligned}
$$

Step 3: Update

$$
\begin{aligned}
\hat{x}_k &= \hat{x}_k^- + K_k[y_k - h_k(\hat{x}_k^-, \hat{f}_{k-1}^*) - D_k^*(\hat{f}_k^* - \hat{f}*_{k-1}], \\
\hat{f}_k^* &= S_k D_k^{*^T} R_k^{-1} (I - H_k K_k)(y_k - h_k(\hat{x}_k^-, \hat{f}_{k-1}^*) + D_k^* \hat{f}_{k-1}^*), \\
P_k &= (I + K_k D_k^* S_k D_k^{*^T} R_k^{-1} H_k)(I - K_k H_k) P_k^{-1}.
\end{aligned}
$$

According to the algorithm discussed above, the seeker signal estimation problem discussed in Chapter 5 has been addressed using the EKF-UI method and then the findings of the simulation are compared to the ESKF approach. Finally, a comparative study of both the methods has been discussed.

6.2 Simulation Results and Discussions

In this module, the findings of the simulations of both ESKF method and EKF-UI method will be compared. The simulation parameters from the previous chapter have been kept unchanged. Although, for the completeness of the chapter, they are discussed in brief once again.

$$
\begin{aligned}
\sigma_v &= 0.2, \\
S_{w1} &= 0.001, \\
S_{w3} &= 0.001.
\end{aligned}
$$

There are two unknown disturbance inputs, i.e., radome error slope and beam pointing error slope. The simulations are performed with two types of nonlinear disturbance inputs. The cases are discussed below.

6.2.1 Sinusoidal input

The disturbance inputs are taken as sinusoids described as

$$R = 0.6 \sin \pi t,$$
$$R^* = 0.6 \cos \pi t.$$

The estimations of the disturbance inputs are given in Fig. 6.1 and Fig. 6.2. In both the figures, the blue line indicates the true value of the inputs, the green line represents the EKF estimate and the red line corresponds to the ESKF estimate. It is clear that the EKF method fails to correctly estimate the disturbance inputs while ESKF estimation is more or less accurate. After a certain time, the EKF estimate diverges from the true value. The most probable reason for this discrepancy is the linearization performed in the EKF algorithm. Since ESKF uses the exact nonlinear system model, it gives accurate and satisfactory results unlike the EKF. Now, the estimation of the system states, i.e., the LOS data are given in Fig. 6.3 and Fig. 6.4. Similar to the previous plots, EKF fails to provide good results but the ESKF estimates the states quite correctly eventually with time. Finally, the mean squared estimation error for LOS rate across 100 Monte Carlo runs have been plotted for the two different filters in Fig. 6.5 and Fig. 6.6. As we can see, for ESKF, the MSE starts from a relatively higher value but decreases with time gradually while the plot diverges for EKF. Hence, it is evident from the simulation findings that the ESKF provides better and more accurate results as compared to the traditional EKF.

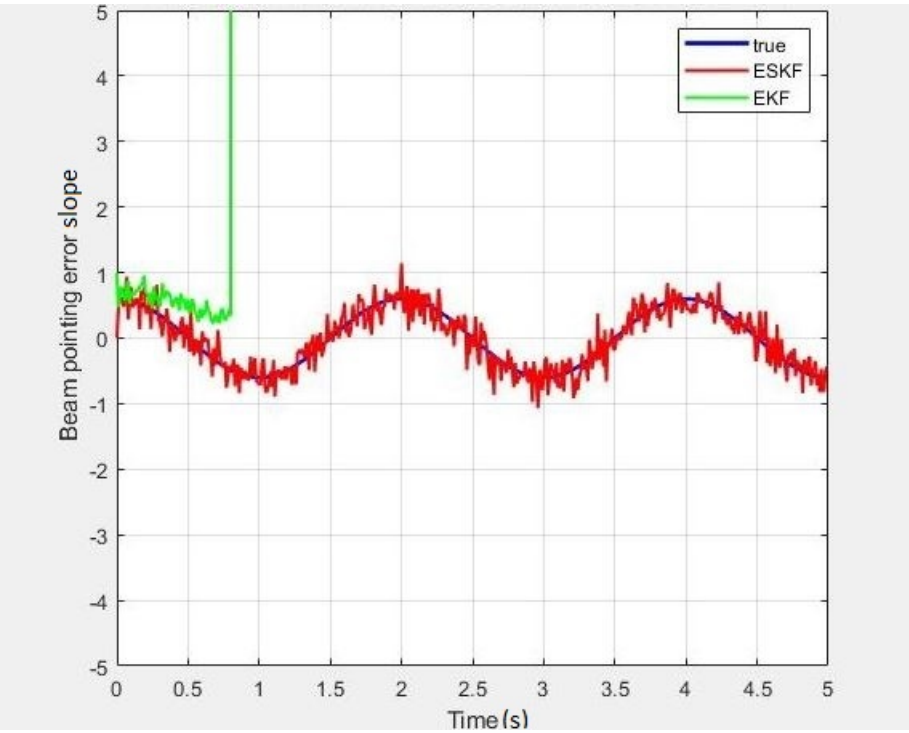

Figure 6.1: True and estimated state of beam pointing error slope for ESKF and EKF

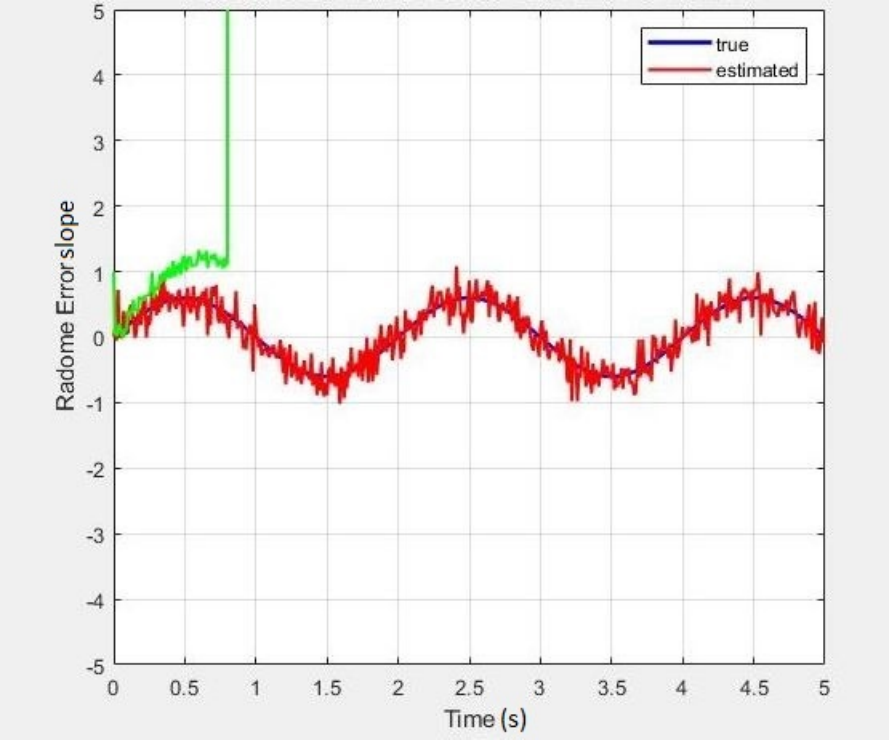

Figure 6.2: True and estimated state of radome error slope for ESKF and EKF

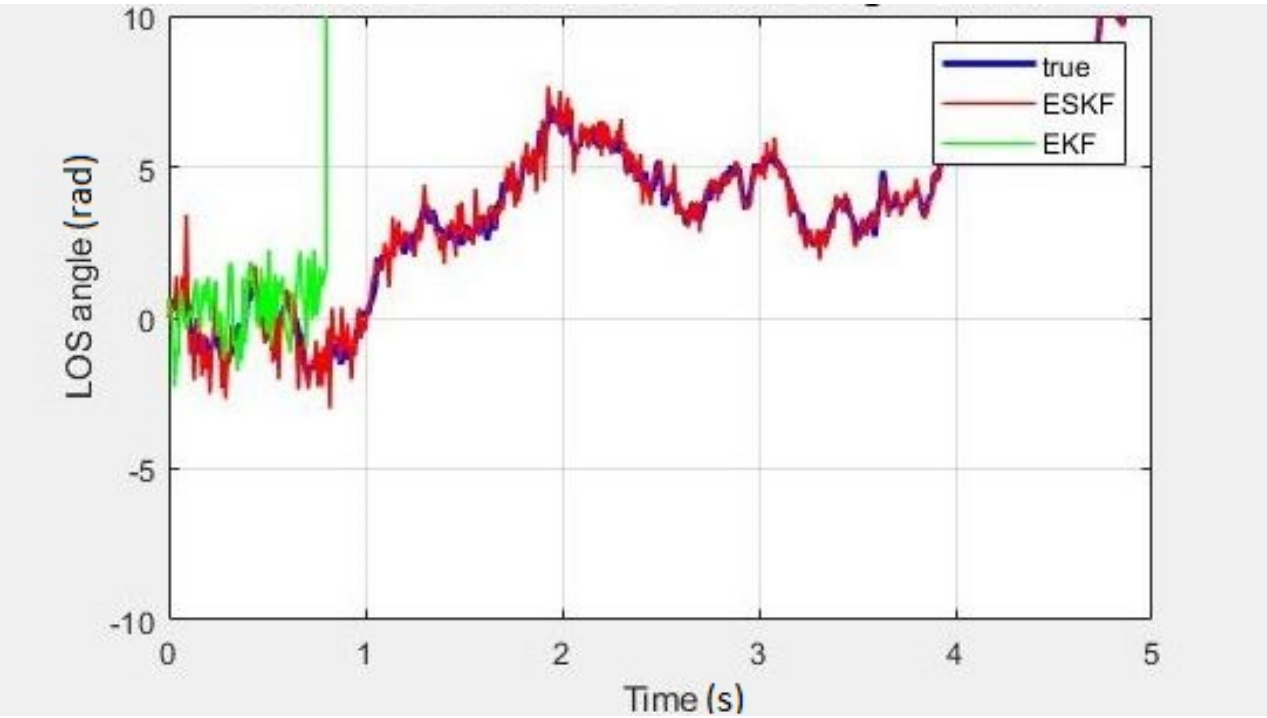

Figure 6.3: True and estimated state of LOS angle for ESKF and EKF

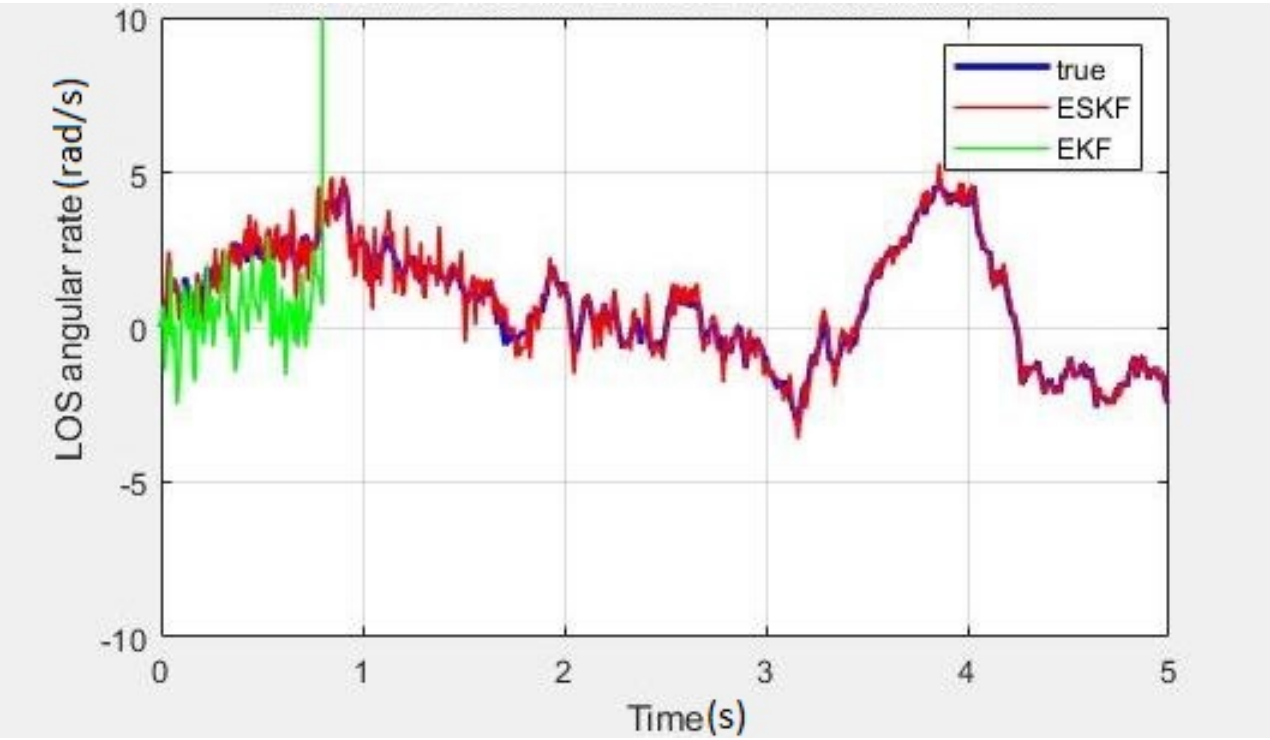

Figure 6.4: True and estimated state of LOS rate for ESKF and EKF

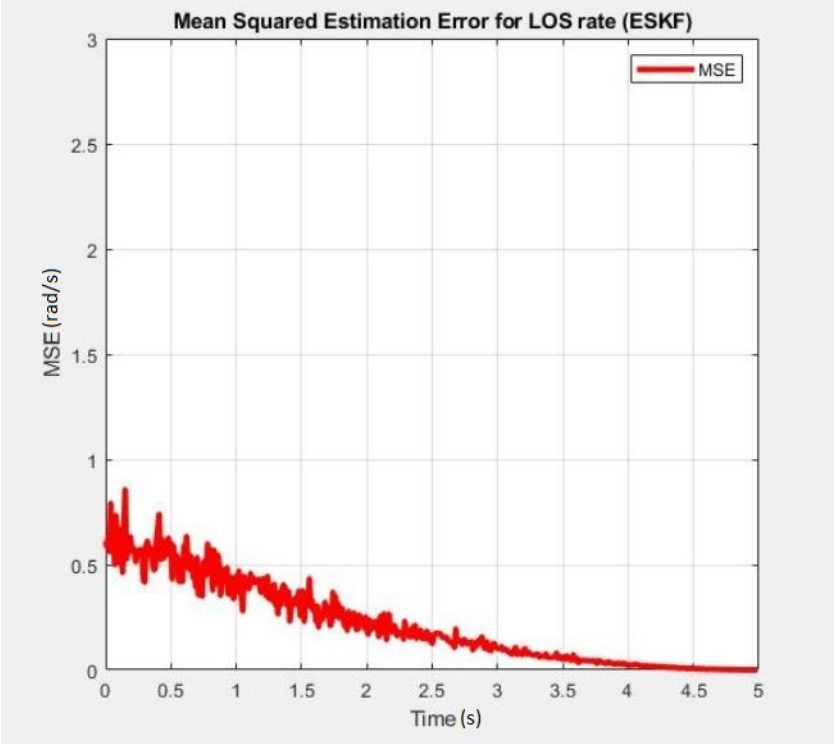

Figure 6.5: Mean squared estimation error for LOS rate for ESKF

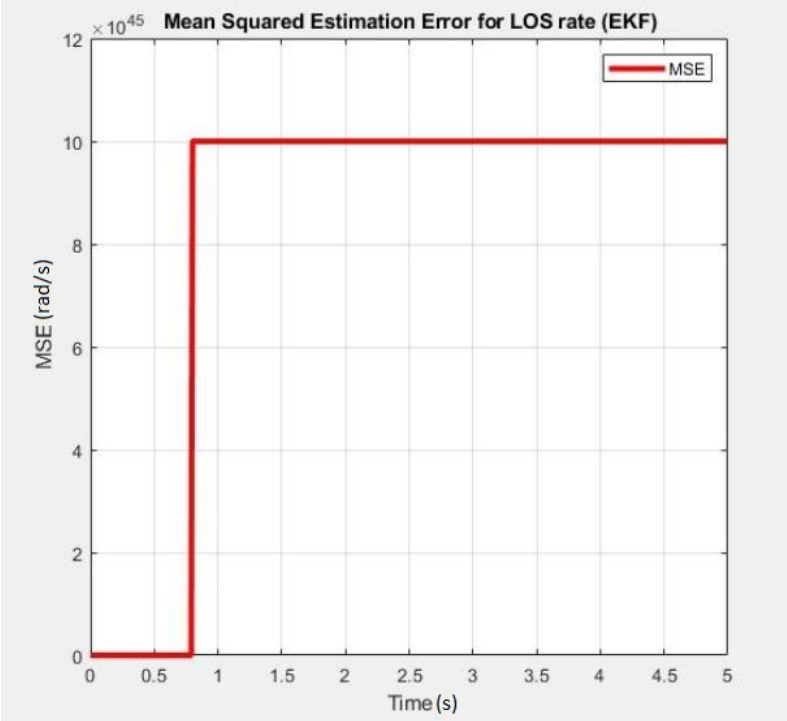

Figure 6.6: Mean squared estimation error for LOS rate for EKF

6.2.2 Chirp Input

A chirp is a special type of signal whose frequency varies with time. The chirp signal that increases in frequency with time is termed up-chirp, while the chirp signal that falls in frequency with time is called down-chirp. A sinusoidal chirp is mathematically expressed as

$$x(t) = \sin 2\pi f(t)t,$$

where $f(t)$ is the chirp waveform's time-dependent frequency. Depending upon the time-dependence of the frequency, a chirp signal can be classified into linear chirp, exponential chirp, hyperbolic chirp etc. The momentary frequency $f(t)$ of a linear chirp changes at a linear rate over time.:

$$f(t) = f_0 + ct,$$

where f_0 represents the initial frequency of the chirp signal and c is the chirp rate which is assumed to be constant. For the purpose of simulation, the chirp frequency has been assumed to be changing from 0.5 Hz to 10.5 Hz and the resulting sinusoidal chirp signals have been used as the disturbance inputs.

$$\begin{aligned} R &= 0.6 \sin 2\pi ft, \\ R^* &= 0.6 \cos 2\pi ft, \\ f &= 0.5 + 2t. \end{aligned}$$

The chirp frequency and the chirp waveform are plotted in Fig. 6.7. The estimations of the disruption inputs for both ESKF and EKF have been depicted in Fig. 6.8 and Fig. 6.9 respectively. From the plots, it is safe to state that the ESKF estimates the unknown disturbance inputs quite correctly while the EKF shows similar results as the previous case, i.e., the response diverges after a certain time. Next, the estimations of the LOS angle and LOS rate are given in Fig. 6.10 and

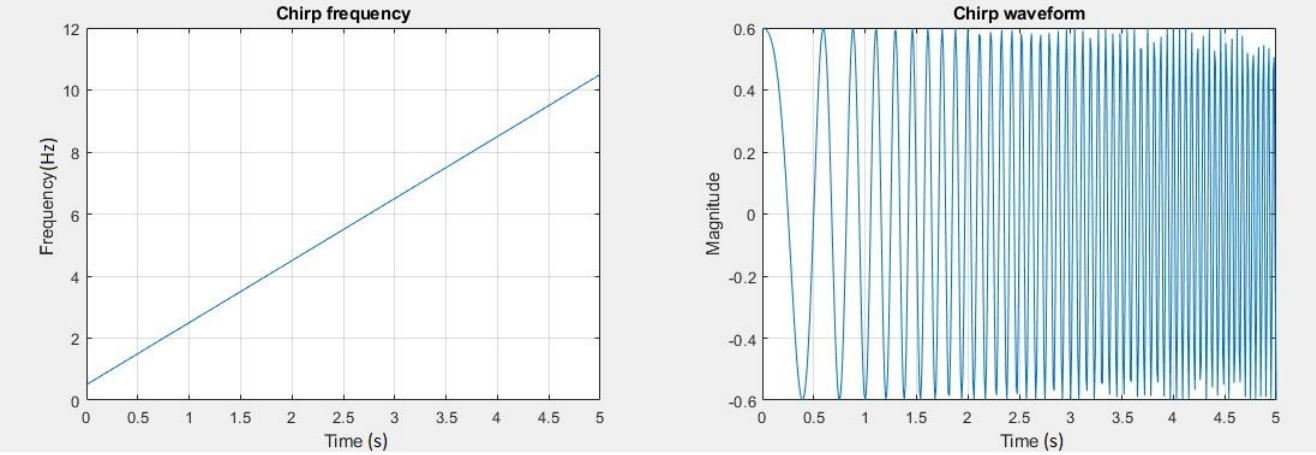

Figure 6.7: Representation of the chirp signal

Fig. 6.11 respectively. As expected, ESKF estimates the system states accurately while the EKF fails to provide good results. Finally, the mean squared estimation errors for LOS rate for 100 Monte Carlo runs for ESKF and EKF are plotted in Fig. 6.12 and Fig. 6.13 respectively. The MSE plot eventually converges with time for ESKF while it diverges for EKF.

The difference between ESKF and the traditional EKF lies in the fact that irrespective of the complexity of the system, linearization is avoided in case of ESKF, thus making it more accurate and less prone to stability issues. The simulation results discussed in this chapter clearly support this fact. The next chapters will dictate the utility of ESKF with more details.

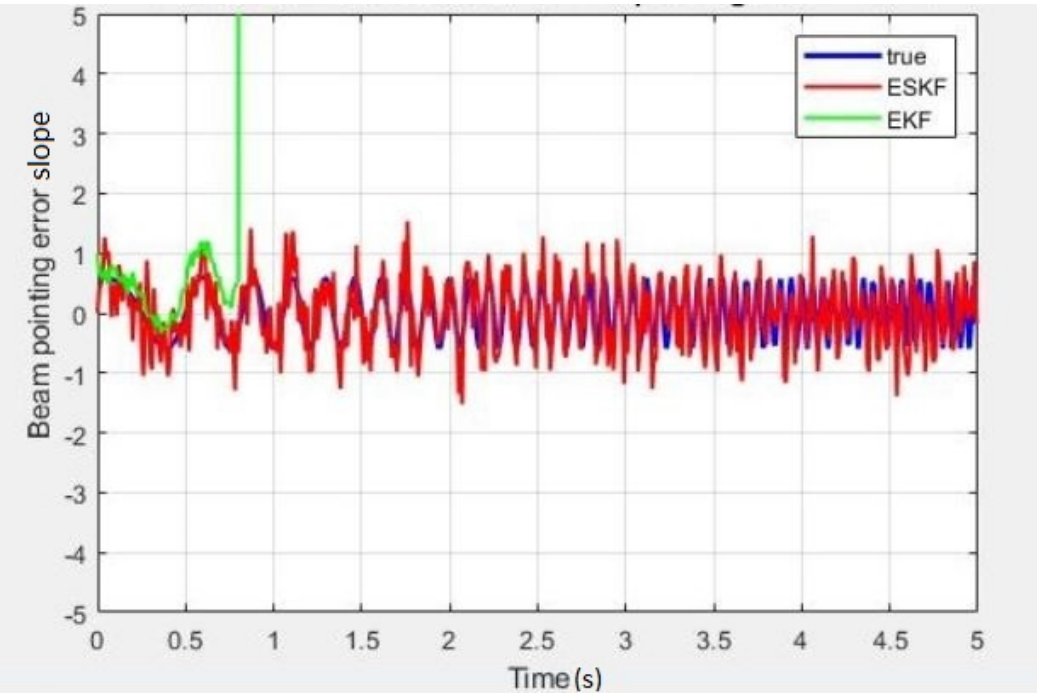

Figure 6.8: True and estimated state of beam pointing error slope for ESKF and EKF in case of chirp input

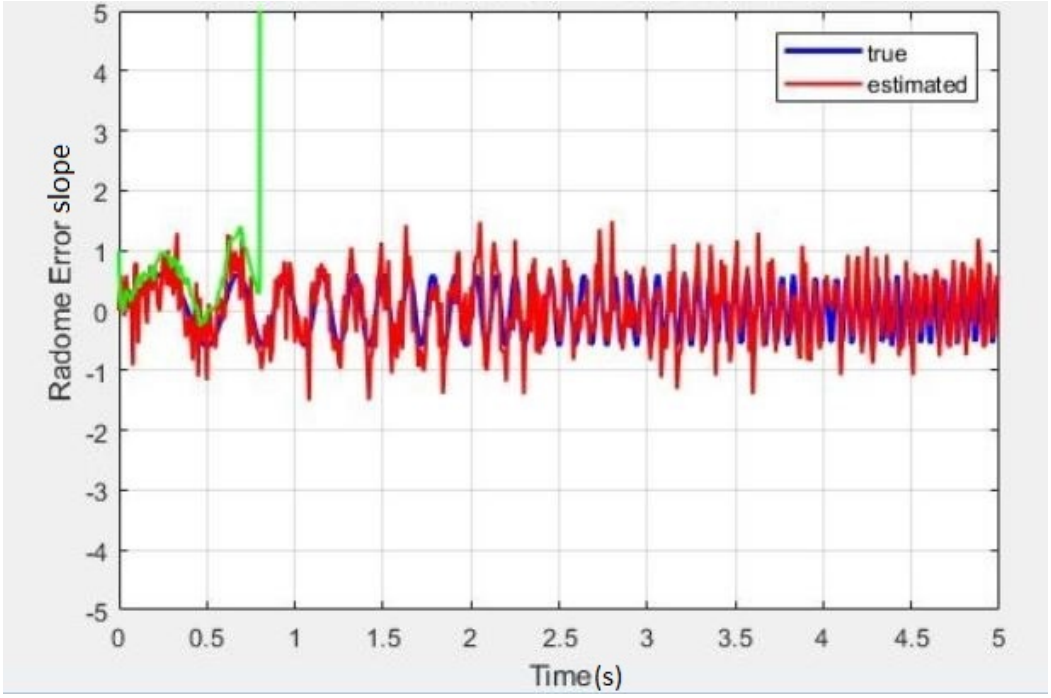

Figure 6.9: True and estimated state of radome error slope for ESKF and EKF in case of chirp input

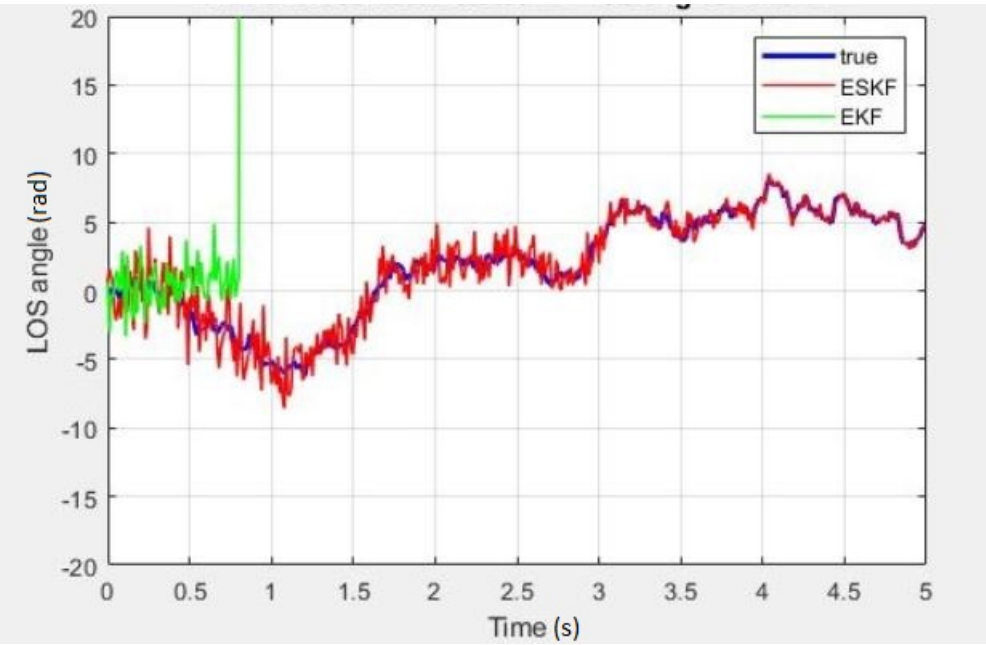

Figure 6.10: True and estimated state of LOS angle for ESKF and EKF in case chirp input

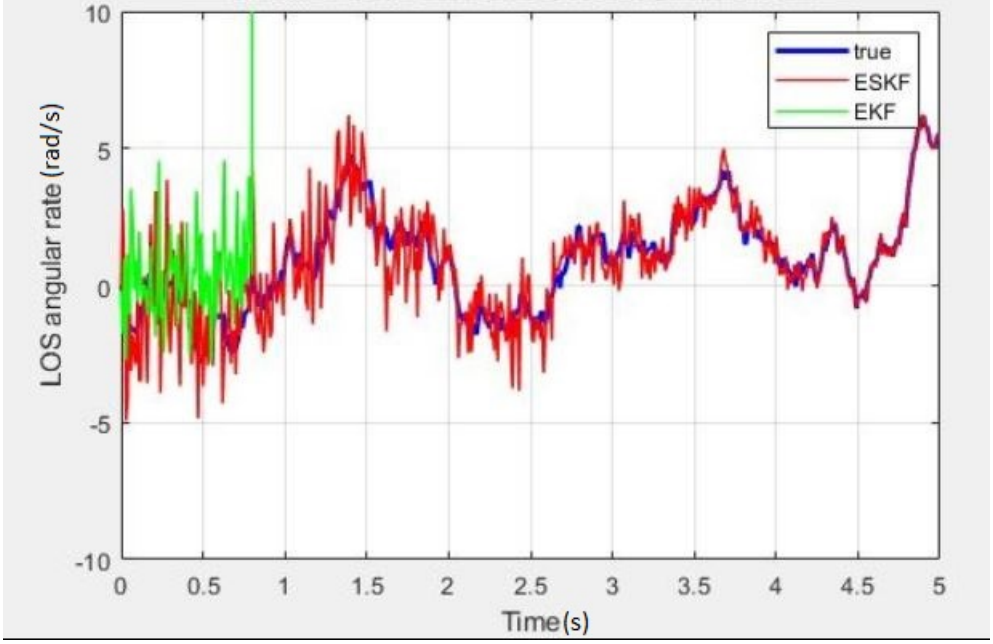

Figure 6.11: True and estimated state of LOS rate for ESKF and EKF in case of chirp input

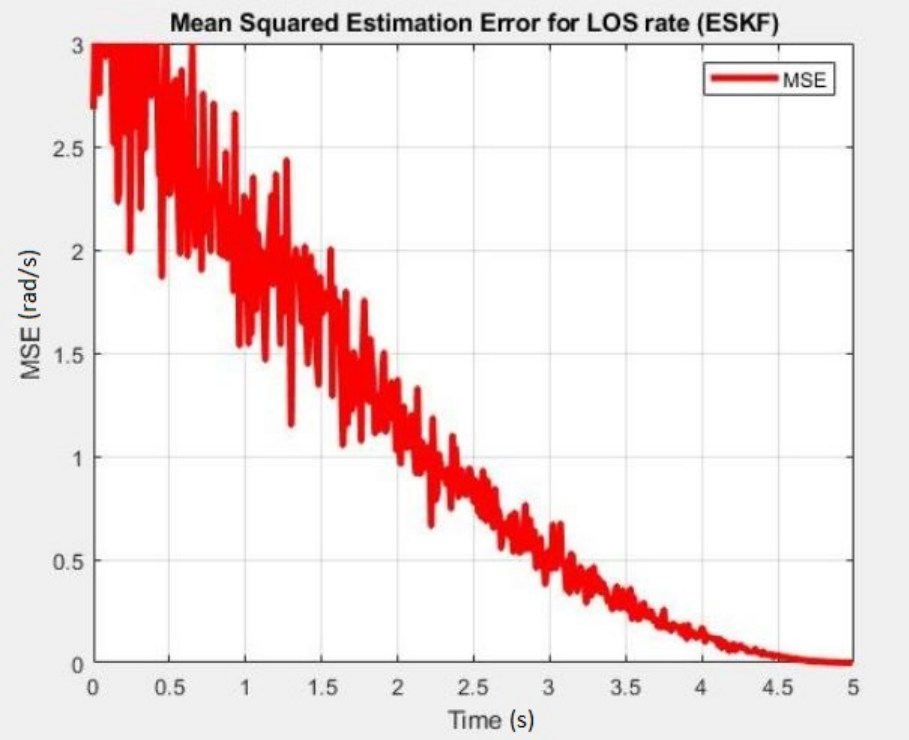

Figure 6.12: Mean squared estimation error for LOS rate for ESKF in case of chirp input

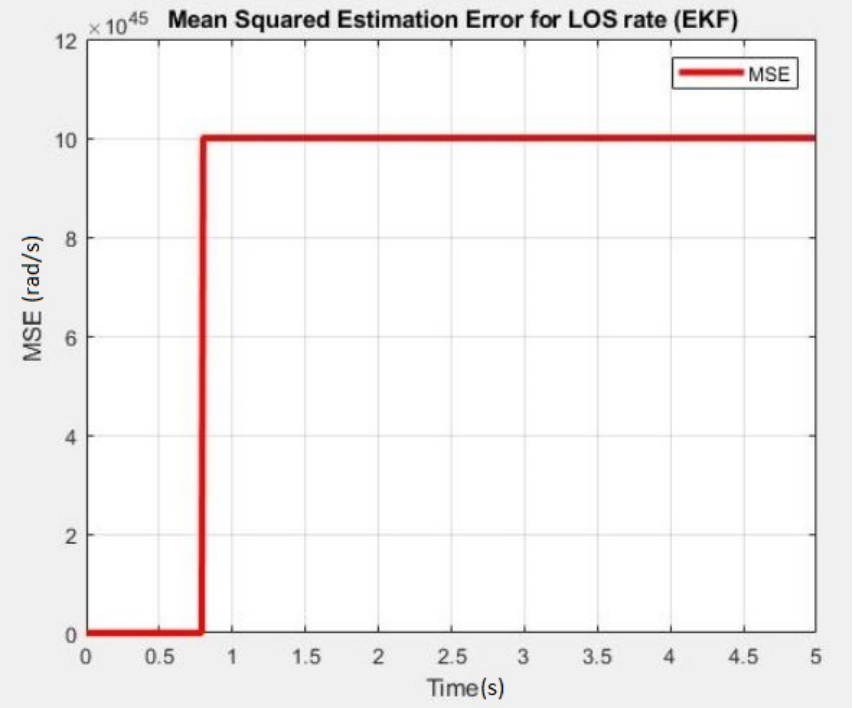

Figure 6.13: Mean squared estimation error for LOS rate for EKF in case of chirp input

Chapter 7

Application of ESKF to a Missile-target Interception Problem with APN Guidance Law

7.1 Problem Statement

In Chapter 5, the ESKF has been applied to the seeker signal estimation problem and the simulation results have been discussed. In Chapter 6, the ESKF has been compared with the traditional EKF with the help of necessary simulation results. In this chapter, the ESKF will be applied to a different guidance problem to further investigate the usefulness of the filter. A simple missile-target engagement problem with APN guidance law has been taken in this chapter. Let us go through the problem statement in a brief.

The graphic representation of the missile and target engagement is depicted in Fig. 7.1 [2]. Here M and T represents the missile and target, V_M and V_T represents their tangential velocities, a_M and a_T are their normal accelerations and θ_M and θ_T are the their flight angles respectively. λ and R are the LOS angle and range respectively. From the geometrical analysis, the following differential equations can be obtained which describe the dynamics of the problem [2].

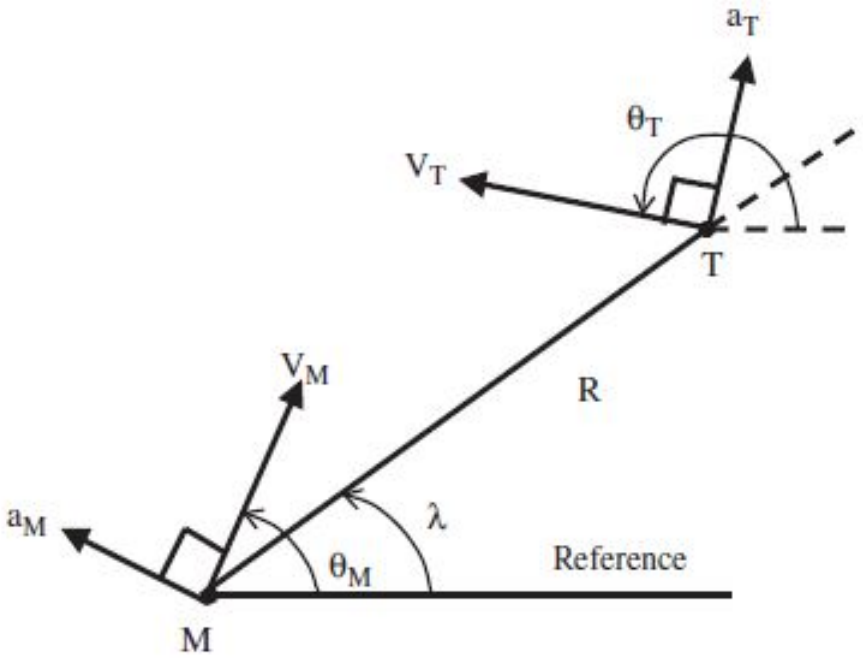

Figure 7.1: Missile-target engagement geometry
[2]

$$\frac{d\lambda}{dt} = \frac{V_T \sin(\theta_T - \lambda) - V_M \sin(\theta_M - \lambda)}{R}, \tag{7.1}$$

$$\frac{dR}{dt} = V_T \cos(\theta_T - \lambda) - V_M \cos(\theta_M - \lambda), \tag{7.2}$$

$$\frac{d\theta_T}{dt} = \frac{a_T}{V_T}, \tag{7.3}$$

$$\frac{d\theta_M}{dt} = \frac{a_M}{V_M}. \tag{7.4}$$

There are two important assumptions related to this problem which are stated below.

(i) The values of the missile's and target's velocities are fixed ($\frac{dV_M}{dt} = 0, \quad \frac{dV_T}{dt} = 0$).
(ii) The flight angles of the interceptor and target are similar and identical to the LOS angle ($\theta_M = \theta_T = \lambda$).

Using the assumption (i) and computing the derivatives of $\dot{R}$ and $\dot{\lambda}$, we get,

$$\frac{d\dot{R}}{dt} = \dot{\lambda}^2 R + a_M \sin(\theta_M - \lambda) - a_T \sin(\theta_T - \lambda), \tag{7.5}$$

$$\frac{d\dot{\lambda}}{dt} = \frac{-2\dot{\lambda}\dot{R} + a_T \cos(\theta_T - \lambda) - a_M \cos(\theta_M - \lambda)}{R}. \tag{7.6}$$

By using assumption (ii) and defining the states and inputs as

$$x_1 = R, \quad x_2 = \dot{R}, \quad x_3 = \lambda \quad x_4 = \dot{\lambda} \quad u = a_M, \quad u^* = a_T.$$

the system's state equations become

$$\dot{x}_1 = x_2, \tag{7.7}$$

$$\dot{x}_2 = x_1 x_4^2 + w_2, \tag{7.8}$$

$$\dot{x}_3 = x_4, \tag{7.9}$$

$$\dot{x}_4 = -2\frac{x_2 x_4}{x_1} + \frac{u^* - u}{x_1} + w_4, \tag{7.10}$$

$$y_1 = x_1 + v_1, \tag{7.11}$$

$$y_2 = x_3 + v_2, \tag{7.12}$$

$$y_3 = x_4 + v_3. \tag{7.13}$$

It should be emphasised that the missile acceleration is treated as a known input, whereas the target acceleration is considered as an unknown input. w_2, w_4 are

the process noise components and v_1, v_2 and v_3 are the measurement noise components. The control input has been computed employing the Augmented Proportional Navigation (APN) guidance law given by

$$a_M = N\hat{V}_c\dot{\hat{\lambda}} + N\frac{\hat{a}_T}{2}.$$

Here N denotes the APN gain and $\hat{V}_c$ represents the closing velocity given by $\hat{V}_c = -\dot{\hat{R}}$ [2]. The target has been assumed to be a random maneuvering target.The target acceleration a_T has been designed as a first order Markov process described as

$$\frac{da_T}{dt} = -\frac{a_T}{\tau} + d(t), \tag{7.14}$$

where $\tau = 0.5$s is the time constant of the actual target model [2] and $d(t)$ is given as

$$d(t) = \begin{cases} 2g & \text{if} \quad n(t) > 0 \\ -2g & \text{if} \quad n(t) < 0 \end{cases} \tag{7.15}$$

where $n(t)$ is the a white noise with known PSD and g is the acceleration due to gravity.

7.2 Simulation Results and Discussions

The Extended State Kalman Filter has been applied to the problem discussed in the previous section. The simulation is performed in MATLAB environment. The filter estimates the unknown input and compensates it and ultimately estimates the system states, i.e., range R, range rate $\dot{R}$, LOS angle λ and LOS rate $\dot{\lambda}$. The initial

conditions of the system are taken as

$$
\begin{aligned}
V_M(0) &= 34.5 \quad m/s, \\
V_T(0) &= 30 \quad m/s, \\
\lambda(0) &= 0 \quad rad, \\
\dot{\lambda}(0) &= 0 \quad rad/s, \\
R(0) &= 90 \quad m, \\
\dot{R}(0) &= -64.5 \quad m/s, \\
\theta_T(0) &= \pi \quad rad, \\
\theta_M(0) &= \pi \quad rad.
\end{aligned}
$$

The process and measurement noise covariance matrices are taken as

$$
Q = \begin{bmatrix} 0.1 & 0 & 0 & 0 \\ 0 & 1 & 0 & 0 \\ 0 & 0 & 0.1 & 0 \\ 0 & 0 & 0 & 1 \end{bmatrix},
$$

$$
R = \begin{bmatrix} 0.1 & 0 & 0 \\ 0 & 0.1 & 0 \\ 0 & 0 & 0.1 \end{bmatrix}.
$$

The prediction of the unspecified input i.e. the target acceleration a_T and the estimation error is depicted in Fig. 7.2 and Fig. 7.3 respectively. Analyzing the plots, it is clear that the ESKF estimates the unknown input quite accurately. Next, the estimation plots of the missile to target range and range rate are depicted in Fig. 7.4 and Fig. 7.5 respectively. Similarly, the estimations of the LOS angle and LOS rate are shown in Fig. 7.6 and Fig. 7.7 respectively. The estimation errors for all the 4 system states are shown in Fig. 7.8. Finally, the mean squared estimation error for LOS rate has been plotted in Fig. 7.9.

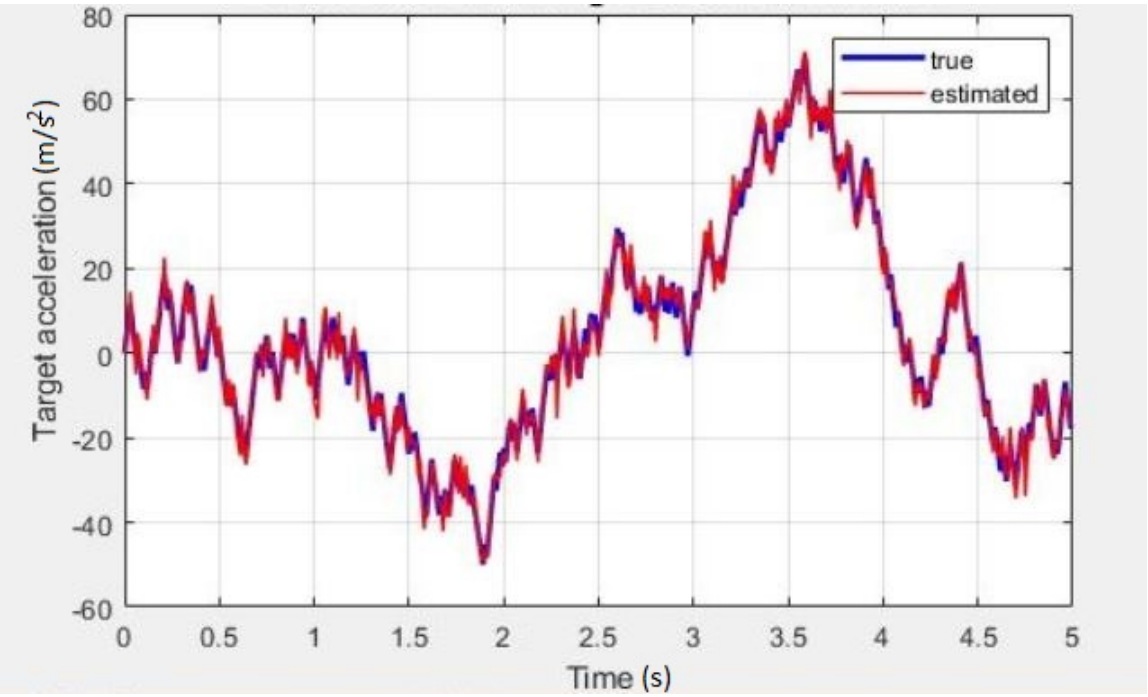

Figure 7.2: True and estimated target acceleration

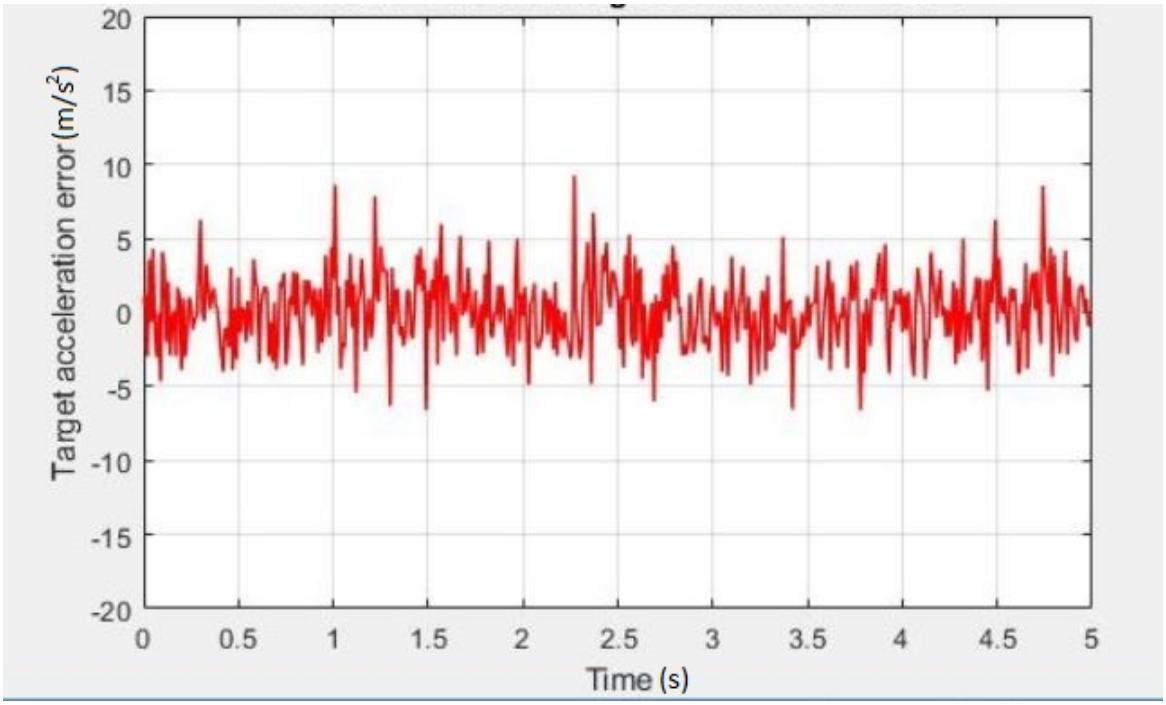

Figure 7.3: Target acceleration error

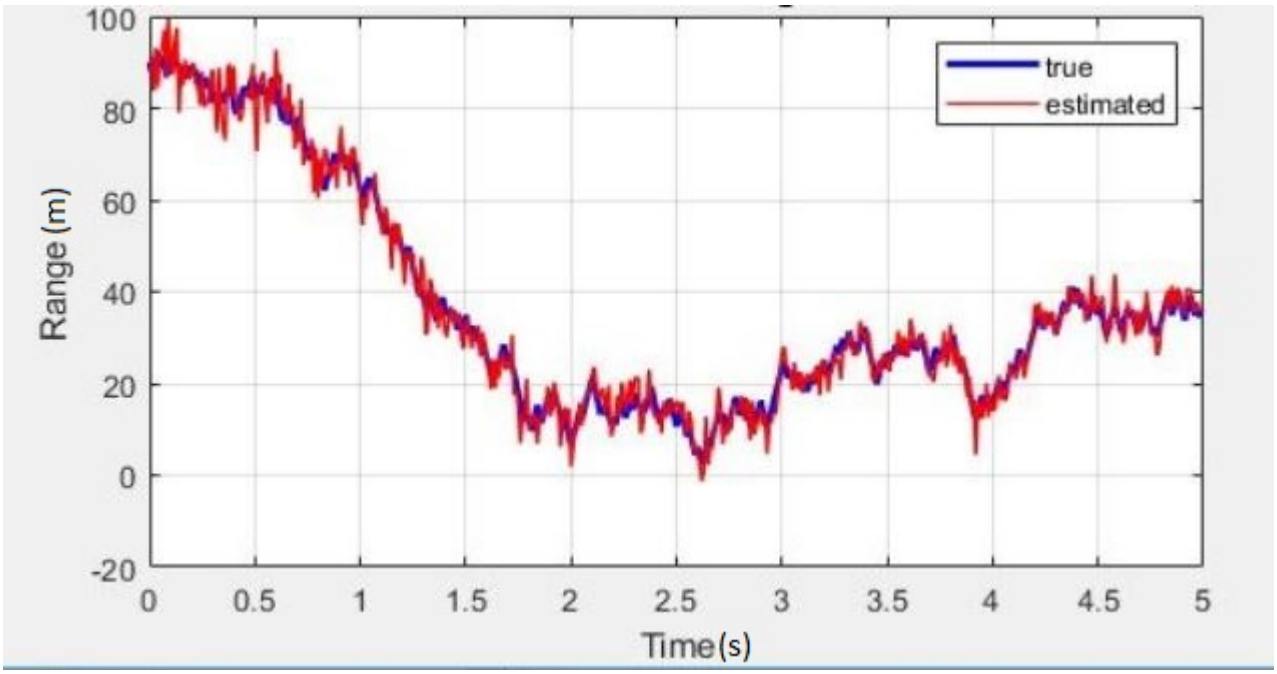

Figure 7.4: True and estimated range

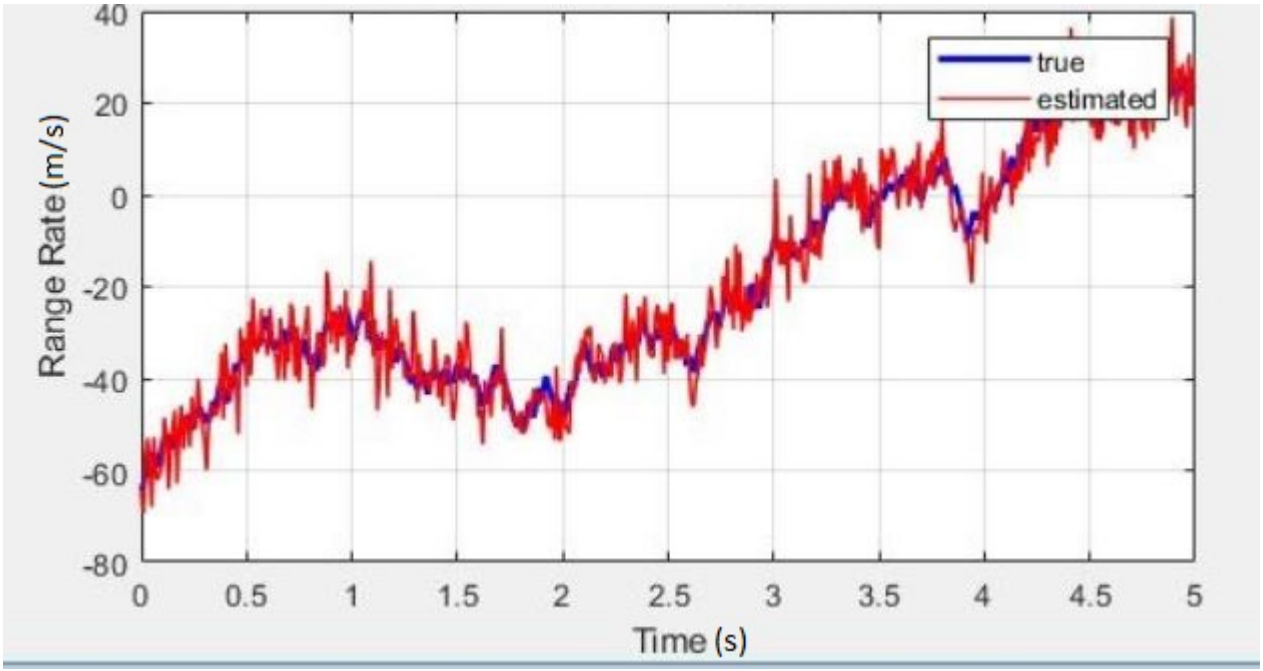

Figure 7.5: True and estimated range rate

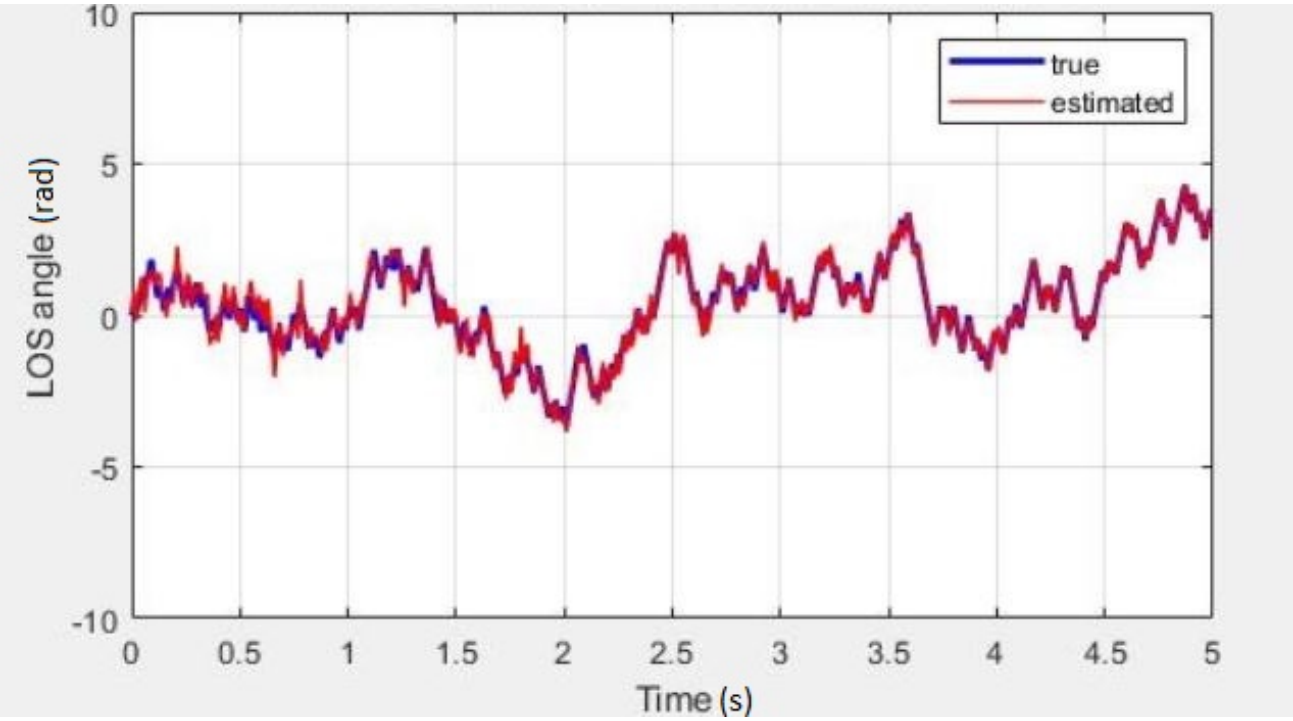

Figure 7.6: True and estimated LOS angle

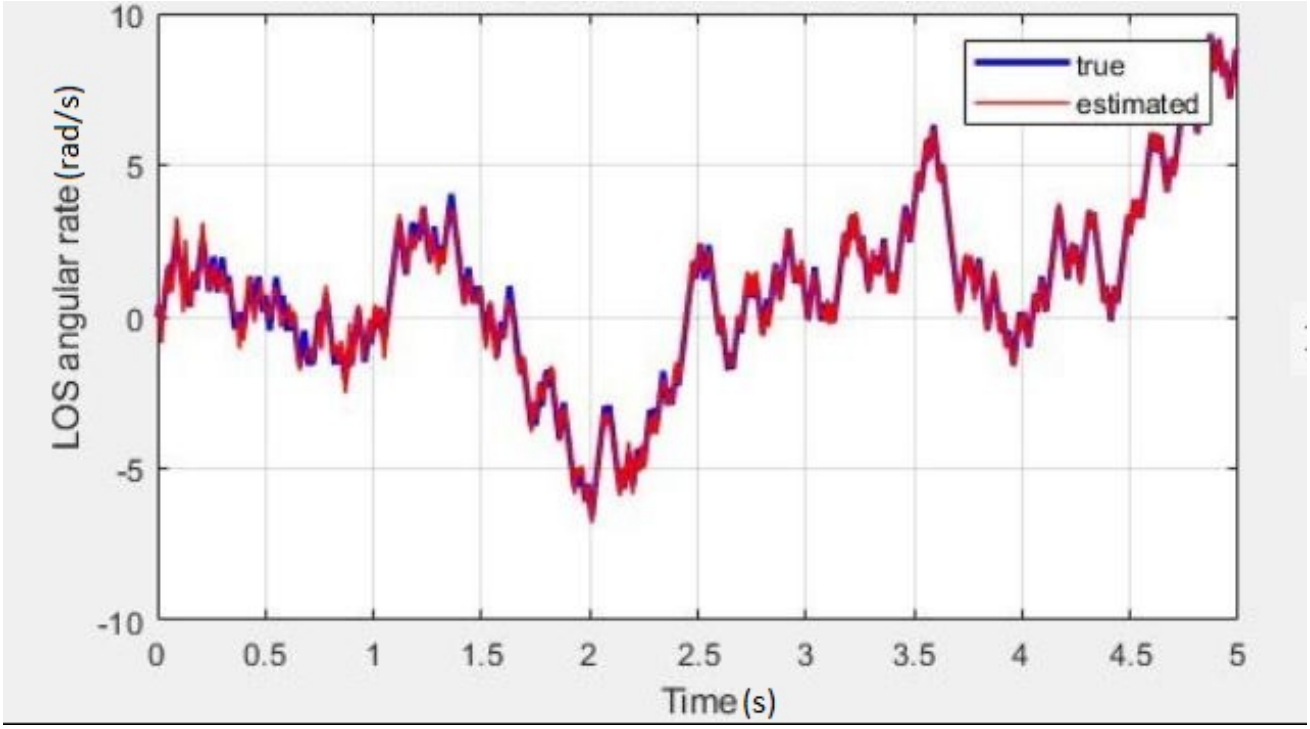

Figure 7.7: True and estimated LOS rate

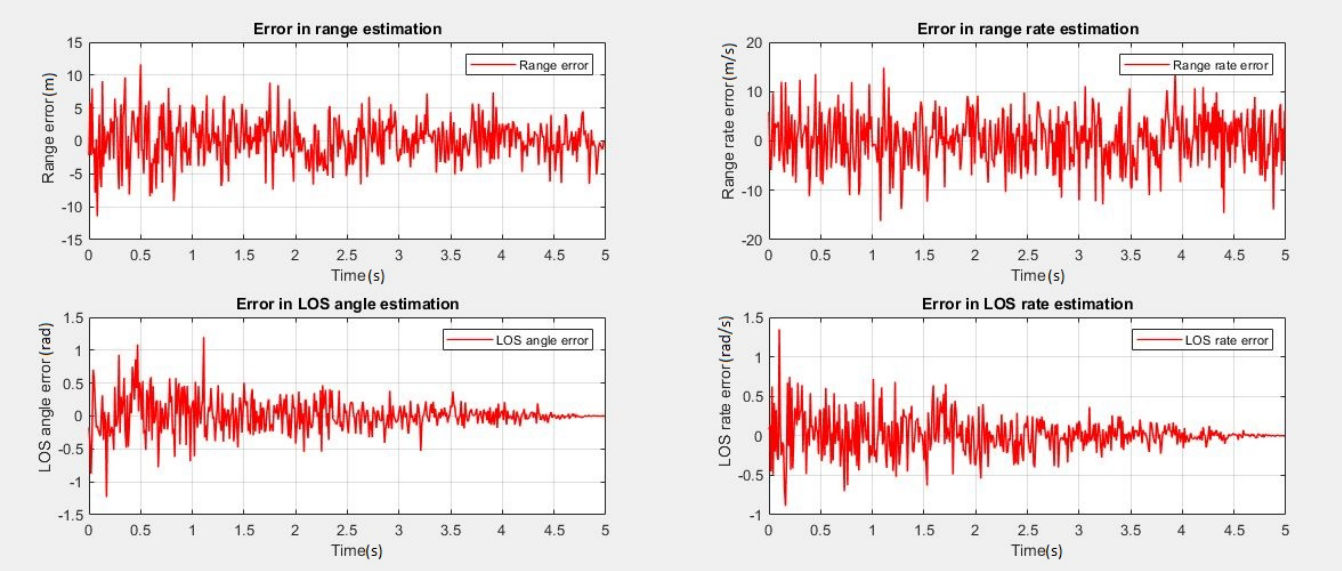

Figure 7.8: Estimation errors for all the states

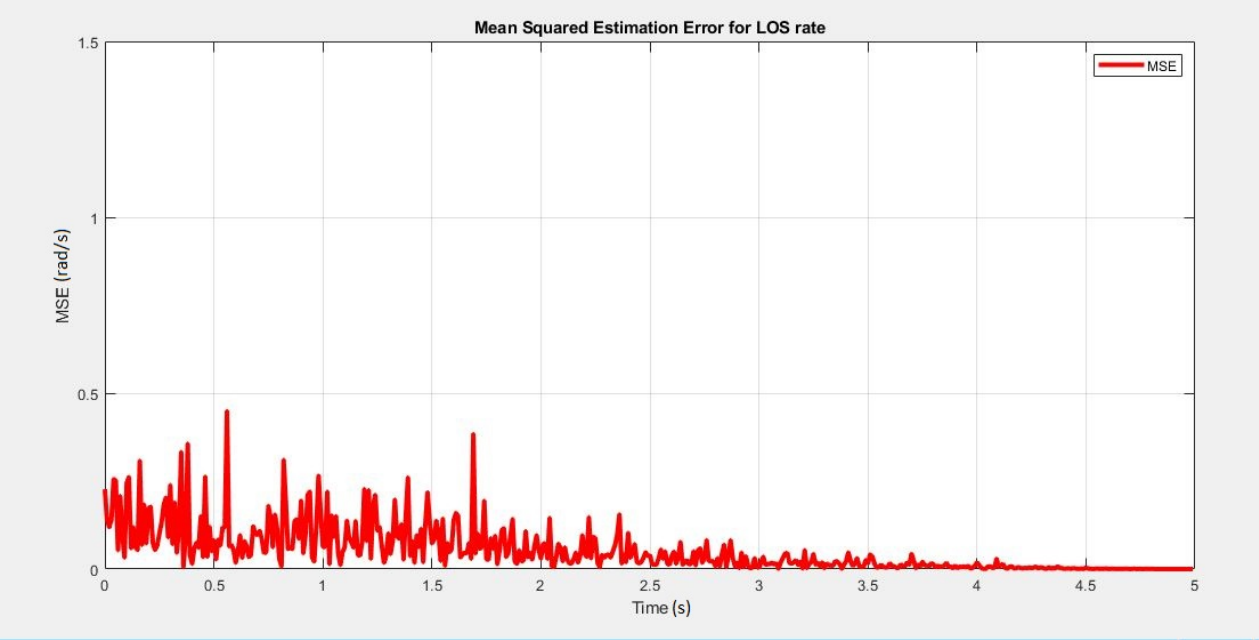

Figure 7.9: Mean squared estimation error for LOS rate

Chapter 8

Robustness Analysis

The term 'robustness' implies the ability to withstand or overcome the adverse conditions or rigorous testing. It is very important for an estimation filter to be robust so that it can compensate the severe noise conditions present in the system. Hence, it is very important to test for robustness of a kalman-type filter under noise unpredictability and model parameter uncertainty. In this chapter, the robustness of the ESKF has been analysed with the help of necessary simulations.

To analyse the robustness of the ESKF, three different cases are considered. The first one involves the nominal noise covariance values as discussed in Chapter 7. For the second and the third case, the measurement noise covariance matrix is kept unchanged but the individual diagonal terms of the process noise covariance matrices are increased to 10 times and 100 times respectively. The noise covariance matrices for the three cases are shown below.

Case I

$$Q = \begin{bmatrix} 0.1 & 0 & 0 & 0 \\ 0 & 1 & 0 & 0 \\ 0 & 0 & 0.1 & 0 \\ 0 & 0 & 0 & 1 \end{bmatrix}, \qquad R = \begin{bmatrix} 0.1 & 0 & 0 \\ 0 & 0.1 & 0 \\ 0 & 0 & 0.1 \end{bmatrix}.$$

Case II

$$Q = \begin{bmatrix} 1 & 0 & 0 & 0 \\ 0 & 10 & 0 & 0 \\ 0 & 0 & 1 & 0 \\ 0 & 0 & 0 & 10 \end{bmatrix}, \qquad R = \begin{bmatrix} 0.1 & 0 & 0 \\ 0 & 0.1 & 0 \\ 0 & 0 & 0.1 \end{bmatrix}.$$

Case III

$$Q = \begin{bmatrix} 10 & 0 & 0 & 0 \\ 0 & 100 & 0 & 0 \\ 0 & 0 & 10 & 0 \\ 0 & 0 & 0 & 100 \end{bmatrix}, \qquad R = \begin{bmatrix} 0.1 & 0 & 0 \\ 0 & 0.1 & 0 \\ 0 & 0 & 0.1 \end{bmatrix}.$$

The mean squared estimation errors across the 100 Monte Carlo runs for the range and the range rate for all the three cases are shown in Fig. 8.1 and 8.2 independently. From the plots, it can be seen that the nature of the MSE curves for all the three cases is similar. Since the initial errors are randomised and the noise covariance values are different, the curves do not coincide. The MSE for the LOS data are depicted in Fig. 8.3 and 8.2. It may be interpreted that the error plots for each of the cases do not differ from the other cases significantly. Therefore, the filter is more or less robust to the change in noise covariances values. Further studies about the robustness of the ESKF can be carried out in future studies.

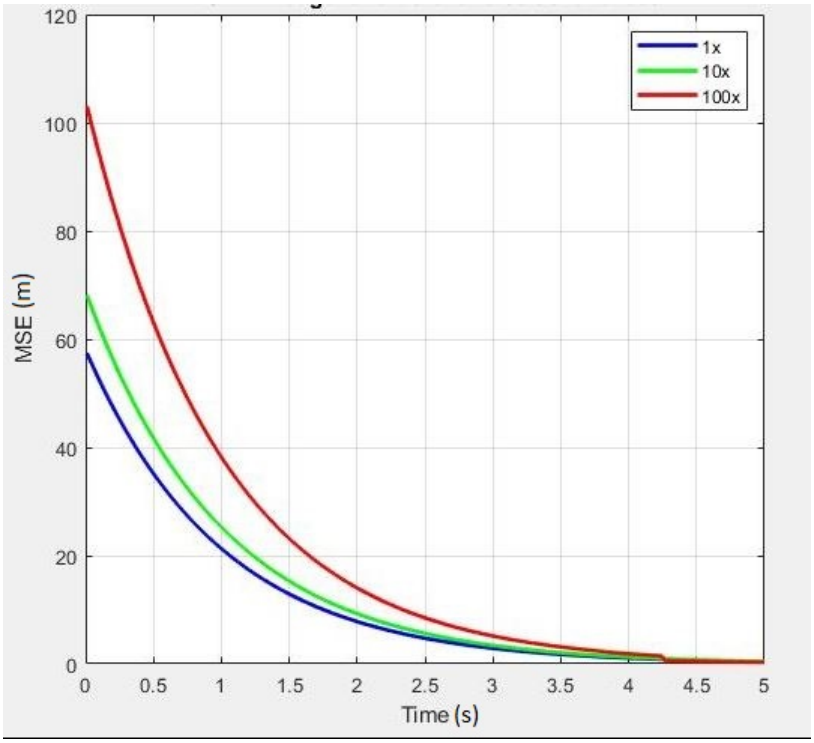

Figure 8.1: Mean squared estimation error for range for three noise levels

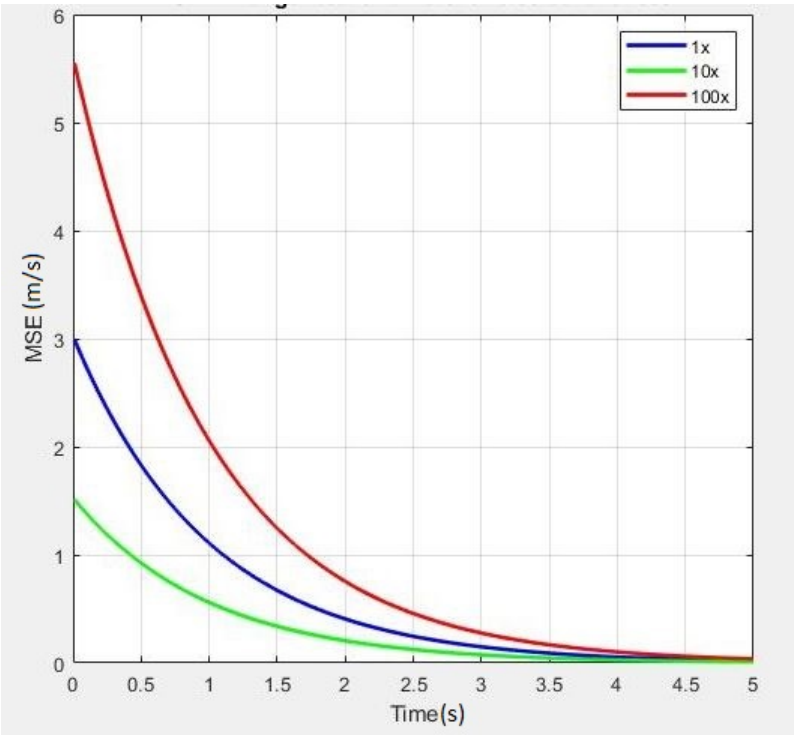

Figure 8.2: Mean squared estimation error for range rate for three noise levels

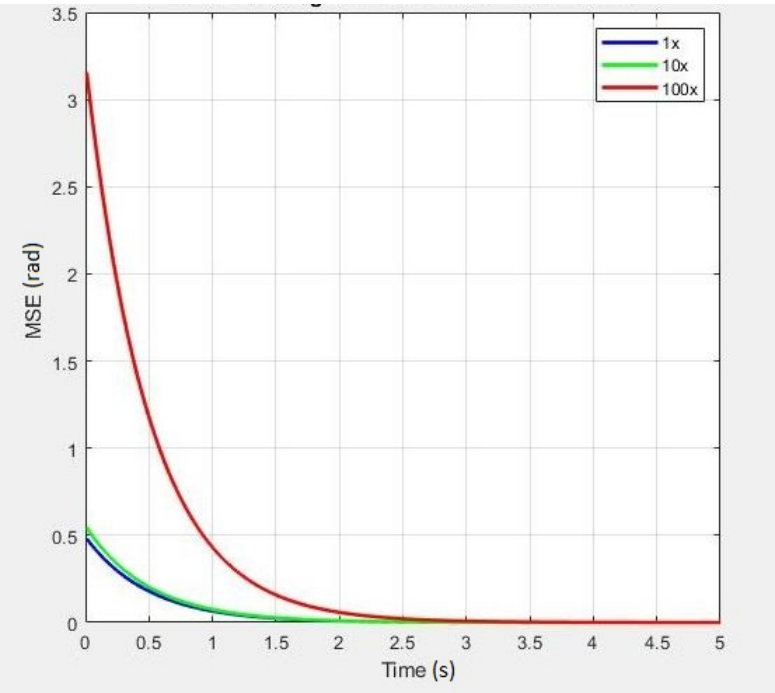

Figure 8.3: Mean squared estimation error for LOS angle for three noise levels

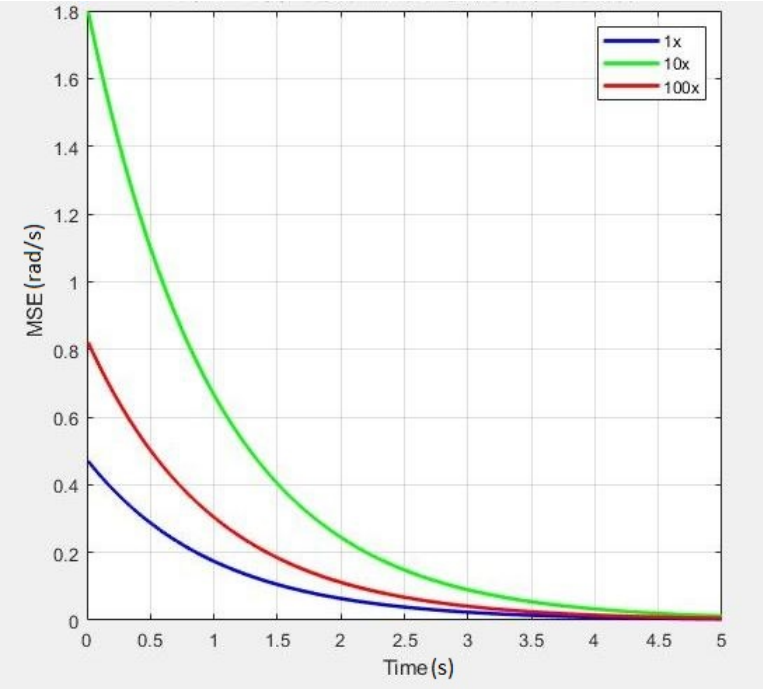

Figure 8.4: Mean squared estimation error for LOS rate for three noise levels

Chapter 9

Concluding Remarks

9.1 Outline of the Work Done

The outline of the work done in this thesis has been divided in certain parts. At first, a deep and detailed literature survey has been done covering all the relevant topics like missile seekers and their classifications, strapdown seekers, guidance loops and parasitic loops, missile seeker geometry, Kalman filter, development in filtering techniques etc. The first part of the literature survey has covered the basics of seekers, mainly the strapdown seeker. A brief description of the same has been provided along with its advantages over the conventional gimbaled seekers. The next part of the literature survey covers the basics of filtering techniques, the development of Kalman filter and the usefulness of these filters in state estimation of the missile.

In Chapter 3, the Extended State Kalman Filter (ESKF) has been discussed in details. The basic concept of ESKF has been discussed along with its advantages over traditional Kalman Filter algorithms. Next, the problem formulation and the design of the ESKF has been discussed. A generalised class of nonlinear time varying uncertain system has been considered and the complete mathematical derivation of the algorithm has been provided. The necessary assumptions have also been stated for performing the mathematical derivation. Finally, at the end of the chapter, the complete steps of the ESKF algorithm have been summarized.

In Chapter 4, the modelling of the seeker has been discussed. The radome error and the beam pointing error which are collectively termed as the DRE problem have been introduced and the impact of partial decoupling of the missile body motion caused by the same has been discussed in brief. Next, the guidance loop has been discussed with the help of a block diagram and each block has been discussed briefly with necessary equations. In the end, the effect of radome and beam pointing error on the guidance block diagram has been discussed and the parasitic loops have been analysed with the transfer function and characteristic equations.

In Chapter 5, the DRE problem discussed previously in Chapter 4 has been addressed using the ESKF. The ESKF algorithm has been applied for the problem and various simulations have been performed to estimate the disturbance inputs and the important states of the system. To test the usefulness of the ESKF, a stronger nonlinearity in the disturbance inputs has also been considered.

In the first section of Chapter 6, the conventional EKF algorithm for unknown inputs has been introduced. Next, the simulation findings of both ESKF and the EKF methods have been compared. Two cases have been considered. In the first case, the disturbance inputs have been considered as sinusoidal and in the next case, they have been taken as linear chirp inputs. Based on the simulation results, a brief comparative discussion between the two methods has also been done. It has been shown that the ESKF provides better results in both the cases mentioned above.

In Chapter 7, the ESKF method has been used to a different problem. A missile-target interception problem has been taken where the target is considered as a randomly maneuvering one. The state equations of the system have been derived and the ESKF algorithm has been applied. Various simulations have been perform to estimate the unknown input and all the states of the system. From the

simulation findings, it has been shown that the ESKF successfully estimates the system states with little error.

In the last chapter, i.e., Chapter 8, the robustness analysis of the ESKF has been performed. The mean squared estimation errors for one particular state in case of three different noise covariance levels have been plotted against each other. It has been concluded that the nature of MSE curves are similar and they do not differ from each other by much. Also, the filter provides stable and bounded results for each noise level.

9.2 Possibility of Future Studies

The current work leads to some possibilities for future studies. They are listed below.

- The ESKF can be applied to the DRE problem using different types of disturbance inputs. Only the sinusoidal and the chirp waveform is used in this study. This will be helpful in proving the utility of the filter [1].
- The usefulness of ESKF can be tested further by applying it to more complex guidance problems.
- In this work, a comparative study between the ESKF and EKF has been done with the help of relevant simulations. In future, a more detailed comparative study may be performed involving different types of kalman like filters including UKF and others.
- There are several mathematical assumptions in the derivation of seeker model that had an effect of making the guidance loop and the parasitic loops less complex. A more detailed and accurate mathematical modelling can be carried out in future that will make the estimate of the seeker signals more precise.

- The robustness analysis can be extended further by designing an adaptive algorithm to update the noise covariance matrices online.

Bibliography

[1] Lin, S.Y., Lin, D. and Wang, W., 2019. A novel online estimation and compensation method for strapdown phased array seeker disturbance rejection effect using extended state Kalman filter. *IEEE Access, 7*, pp.172330-172340.

[2] Madyastha, V.K., 2005. *Adaptive estimation for control of uncertain nonlinear systems with applications to target tracking*. Georgia Institute of Technology.

[3] Sutton, G.P., 1955. History, Problems, and Status of Guided Missiles. *Journal of Jet Propulsion, 25(11)*, pp.615-622.

[4] Garnell, P., East, D.J. and Siouris, G.M., 1979. Guided weapon control systems. *IEEE Transactions on Systems, Man, and Cybernetics, 9(11)*, pp.740-741.

[5] Siouris, G.M., 2004. *Missile guidance and control systems*. Springer Science Business Media.

[6] Reif, K., 2019. National missile defense set back. *Arms Control Today, 49(6)*, pp.26-28.

[7] Wittenberg, P.S., Boeing Co, 2017. *Short-range point defense radar*. U.S. Patent 9,810,774.

[8] Nielsen, J., 1988. *Missile aerodynamics*. American Institute of Aeronautics and Astronautics, Inc.

[9] Pastrick, H.L., Seltzer, S.M. and Warren, M.E., 1981. Guidance laws for short-range tactical missiles. *Journal of Guidance and Control, 4(2)*, pp.98-108.

[10] Laur, T.M., 2015. *Encyclopedia of modern US military weapons*. ACristian.

[11] Evans, S.G. and Delaney, K.B., 2018. The V1 (Flying Bomb) attack on London (1944–1945); the applied geography of early cruise missile accuracy. *Applied geography*, 99, pp.44-53.

[12] Jalil, G.Y., 2015. Indian Missile Defence Development: Implications for Deterrence Stability in South Asia. *Strategic Studies, 35(2)*.

[13] Moon, K., Kwon, H., Ryoo, C.K. and Sim, H., 2018, July. Trajectory estimation for a ballistic missile in ballistic phase using IR images. In *2018 9th International Conference on Mechanical and Aerospace Engineering (ICMAE)* (pp. 173-177). IEEE.

[14] Singh, N.K., Bhaumik, S. and Bhattacharya, S., 2016, January. A comparison of several nonlinear filters for ballistic missile tracking on re-entry. In *2016 IEEE First International Conference on Control, Measurement and Instrumentation (CMI)* (pp. 459-463). IEEE.

[15] Stein, R. and Carlini, J., 2017. *Defense Science Board Task Force on Defense Strategies for Advanced Ballistic and Cruise Missile Threats*. DEFENSE SCIENCE BOARD WASHINGTON DC WASHINGTON DC United States.

[16] Etkin, B., 2012. *Dynamics of atmospheric flight*. Courier Corporation.

[17] Goldstein, H., 2011. *Classical mechanics*. Pearson Education India.

[18] Lanczos, C., 2012. *The variational principles of mechanics*. Courier Corporation.

[19] Nicolai, L.M., 1975. *Fundamentals of aircraft design*. Nicolai.

[20] Roskam, J., 1982. *Airplane Flight Dynamics and Automatic Flight Controls: Chapters 1 Through 6, Rigid Airplane Flight Dynamics (open Loop)*. Roskam Aviation and Engineering Corporation.

[21] Siouris, G., 1993. *Aerospace avionics systems: a modern synthesis*.

[22] Willman, W.W., 1988. Effects of strapdown seeker scale-factor uncertainty on optimal guidance. *Journal of Guidance, Control, and Dynamics, 11(3)*, pp.199-206.

[23] Mehra, R.K. and Ehrich, R.D., 1984, December. Air-to-air missile guidance for strapdown seekers. In *The 23rd IEEE Conference on Decision and Control* (pp. 1109-1115). IEEE.

[24] Du, Y.L., Xia, Q.L. and Guo, T., 2010, August. Study on stability of strapdown seeker scale factor error parasitical loop. In *2010 International Conference on Computer, Mechatronics, Control and Electronic Engineering* (Vol. 6, pp. 55-58). IEEE.

[25] Kim, T.H., Park, B.G., Kwon, H.H., Kim, Y.H. and Tahk, M.J., 2011. Stability Analysis of Missiles with Strapdown Seeker. *Journal of the Korean Society for Aeronautical Space Sciences, 39(4)*, pp.332-340.

[26] Jianmei, S., Gaohua, C., Xianxiang, C. and Lixia, K., 2012. Stability region analysis of the parasitic loop of the semi-strapdown homing seeker. *Proceedings of the Institution of Mechanical Engineers, Part I: Journal of Systems and Control Engineering, 226(4)*, pp.550-562.

[27] Jianmei, S., Gaohua, C., Lixia, K. and Jianhua, F., 2012. Precision analysis of the semi-strapdown homing guided system. In *AIAA Guidance, Navigation, and Control Conference* (p. 4687).

[28] Rui, B.A.I., Qun-li, X.I.A., Xiao, D.U. and Tian-yu, L.U., 2017. Test of Parasitic Loop Quality of Strapdown Seeker. *Acta Armamentarii, 38(3)*, p.494.

[29] Bai, R., Xia, Q. and Du, X., 2017. The study of guidance performance of a phased array seeker with platform. *Optik, 132*, pp.9-23.

[30] Kim, D., Park, W. and Ryoo, C.K., 2013. Look-Angle-Control Guidance for Missiles with Strapdown Seeker. *Journal of Institute of Control, Robotics and Systems, 19(3)*, pp.275-280.

[31] Lee, C.H., Hyun, C., Lee, J.G., Choi, J.Y. and Sung, S., 2013. A hybrid guidance law for a strapdown seeker to maintain lock-on conditions against high speed targets. *Journal of Electrical Engineering and Technology, 8(1)*, pp.190-196.

[32] Hong, J.H. and Ryoo, C.K., 2014, September. Compensation of parasitic effect in homing loop with strapdown seeker via PID control. In 2014 *11th International Conference on Informatics in Control, Automation and Robotics (ICINCO)* (Vol. 1, pp. 711-717). IEEE.

[33] Mehra, R.K. and Ehrich, R.D., 1984, December. Air-to-air missile guidance for strapdown seekers. In *The 23rd IEEE Conference on Decision and Control* (pp. 1109-1115). IEEE.

[34] Jang, S.A., Ryoo, C.K., Choi, K. and Tahk, M.J., 2008, August. Guidance algorithms for tactical missiles with strapdown seeker. In *2008 SICE Annual Conference* (pp. 2616-2619). IEEE.

[35] Lee, C.H., Hyun, C., Lee, J.G., Choi, J.Y. and Sung, S., 2013. A hybrid guidance law for a strapdown seeker to maintain lock-on conditions against high speed targets. *Journal of Electrical Engineering and Technology, 8(1)*, pp.190-196.

[36] Murtaugh, S.A. and Criel, H.E., 1966. Fundamentals of proportional navigation. *IEEE spectrum, 3(12)*, pp.75-85.

[37] Yuan, P.J. and Chern, J.S., 1992. Ideal proportional navigation. *Journal of Guidance, Control, and Dynamics, 15(5)*, pp.1161-1165.

[38] Yang, C.D., Hsiao, F.B. and Yeh, F.B., 1989. Generalized guidance law for homing missiles. *IEEE Transactions on Aerospace and Electronic Systems, 25(2)*, pp.197-212.

[39] Cloutier, J.R., Evers, J.H. and Feeley, J.J., 1989. Assessment of air-to-air missile guidance and control technology. *IEEE Control systems magazine, 9(6)*, pp.27-34.

[40] Zarchan, P., 2012. *Tactical and strategic missile guidance*. American Institute of Aeronautics and Astronautics, Inc..

[41] Shukla, U.S. and Mahapatra, P.R., 1990. The proportional navigation dilemma-pure or true?. *IEEE Transactions on Aerospace and Electronic Systems, 26(2)*, pp.382-392.

[42] Xin, M., Balakrishnan, S. and Ohlmeyer, E., 2006, August. Guidance law design for missiles with reduced seeker field-of-view. In *AIAA Guidance, Navigation, and Control Conference and Exhibit* (p. 6085).

[43] Sang, D., Ryoo, C.K., Song, K.R. and Tahk, M.J., 2008, August. A guidance law with a switching logic for maintaining seeker's lock-on for stationary targets. In AIAA Guidance, Navigation and Control Conference and Exhibit (p. 6497).

[44] Wang, C., Liu, Y. and Song, J., 2016, November. A hardware-in-the-loop simulation for LOS rate estimation of strapdown seeker based on EKF. In *2016 14th International Conference on Control, Automation, Robotics and Vision (ICARCV)* (pp. 1-5). IEEE.

[45] Julier, S.J., Uhlmann, J.K. and Durrant-Whyte, H.F., 1995, June. A new approach for filtering nonlinear systems. In *Proceedings of 1995 American Control Conference-ACC'95* (Vol. 3, pp. 1628-1632). IEEE.

[46] Julier, S. and Uhlmann, J.K., 1996. *A general method for approximating nonlinear transformations of probability distributions*.

[47] Zhang, G.J., Yao, Y. and Ma, K.M., 2005, August. Line of sight rate estimation of strapdown imaging guidance system based on unscented Kalman filter. In *2005 International Conference on Machine Learning and Cybernetics* (Vol. 3, pp. 1574-1578). IEEE.

[48] Sadhu, S. and Ghoshal, T.K., 2010. Sight line rate estimation in missile seeker using disturbance observer-based technique. *IEEE Transactions on Control Systems Technology, 19(2)*, pp.449-454.

[49] Wang, P. and Zhang, K., 2014, July. Research on line-of-sight rate extraction of strapdown seeker. In *Proceedings of the 33rd Chinese Control Conference* (pp. 859-863). IEEE.

[50] Waldmann, J., 2002. Line-of-sight rate estimation and linearizing control of an imaging seeker in a tactical missile guided by proportional navigation. *IEEE Transactions on control systems technology, 10(4)*, pp.556-567.

[51] Bai, W., Xue, W., Huang, Y. and Fang, H., 2018. On extended state based Kalman filter design for a class of nonlinear time-varying uncertain systems. *Science China Information Sciences, 61(4)*, pp.1-16.

[52] Nesline, F.W. and Zarchan, P., 1984. Miss distance dynamics in homing missiles. In *17th Fluid Dynamics, Plasma Dynamics, and Lasers Conference* (p. 1844).

[53] Du, X. and Xia, Q., 2017. Research on strap-down seeker guidance information for rolling interceptor. *Optik, 129*, pp.183-199

[54] Raj, K.D.S. and Ganesh, I.S.S., 2015, April. Estimation of line-of-sight rate in a homing Missile Guidance loop using optimal filters. In *2015 International Conference on Communications and Signal Processing (ICCSP)* (pp. 0398-0402). IEEE.